

Nucleosynthesis of binary-stripped stars.

R. FARMER,¹ E. LAPLACE,^{2,3} JING-ZE MA,¹ S. E. DE MINK,^{1,3} AND S. JUSTHAM^{4,5,3,1}

¹*Max-Planck-Institut für Astrophysik, Karl-Schwarzschild-Straße 1, 85741 Garching, Germany*

²*Heidelberger Institut für Theoretische Studien, Schloss-Wolfsbrunnengasse 35, 69118 Heidelberg, Germany*

³*Anton Pannekoek Institute for Astronomy and GRAPPA, University of Amsterdam, NL-1090 GE Amsterdam, The Netherlands*

⁴*School of Astronomy & Space Science, University of the Chinese Academy of Sciences, Beijing 100012, China*

⁵*National Astronomical Observatories, Chinese Academy of Sciences, Beijing 100012, China*

(Dated: March 9, 2023)

ABSTRACT

The cosmic origin of the elements, the fundamental chemical building blocks of the Universe, is still uncertain. Binary interactions play a key role in the evolution of many massive stars, yet their impact on chemical yields is poorly understood. Using the MESA stellar evolution code we predict the chemical yields ejected in wind mass loss and the supernovae of single and binary-stripped stars. We do this with a large 162 isotope nuclear network at solar-metallicity. We find that binary-stripped stars are more effective producers of the elements than single stars, due to their increased mass loss and an increased chance to eject their envelopes during a supernova. This increased production by binaries varies across the periodic table, with F and K being more significantly produced by binary-stripped stars than single stars. We find that the $^{12}\text{C}/^{13}\text{C}$ could be used as an indicator of the conservativeness of mass transfer, as ^{13}C is preferentially ejected during mass transfer while ^{12}C is preferentially ejected during wind mass loss. We identify a number of gamma-ray emitting radioactive isotopes that may be used to help constrain progenitor and explosion models of core-collapse supernovae with next-generation gamma-ray detectors. For single stars we find ^{44}V and ^{52}Mn are strong probes of the explosion model, while for binary-stripped stars it is ^{48}Cr . Our findings highlight that binary-stripped stars are not equivalent to two single stars and that detailed stellar modelling is needed to predict their final nucleosynthetic yields.

1. INTRODUCTION

The origin of the elements is an unsolved problem (Arnould & Takahashi 1999; José & Iliadis 2011; Diehl et al. 2022). Massive stars play a role in the formation of the elements through their ejection of processed material in their winds (Kudritzki & Puls 2000; Vink et al. 2001; Crowther 2007; Smith 2014) and the ejecta from core-collapse (CC) supernovae (Maeder 1992; Rauscher et al. 2002; Heger et al. 2003).

Most massive stars have been found to be born with at least one companion (Abt 1983; Mason et al. 2009), and the majority are expected to undergo at least one phase of mass transfer (Sana et al. 2012; Moe & Di Stefano 2017). During mass transfer the majority of the hydrogen-rich envelope of the star (Kippenhahn & Weigert 1967; Yoon et al. 2010; Götzberg et al. 2017) may

be removed and some fraction of it accreted onto its companion. This mass transfer alters both stars' subsequent evolution (Podsiadlowski et al. 1992; Brown et al. 1996; Wellstein & Langer 1999; Eldridge et al. 2008; Langer 2012; de Mink et al. 2013) and final chemical element production (Braun & Langer 1995a; Laplace et al. 2021; Farmer et al. 2021). Binarity has also been used to explain the composition of carbon and s-element enhanced metal-poor (CEMP-s) stars, by requiring efficient wind mass transfer in the system (Abate et al. 2015).

Explosive nucleosynthesis, during core-collapse (CC) supernova (SN), in massive stars has been well studied for single star objects (Woosley et al. 1993; Heger et al. 2001; Heger & Woosley 2002; Heger et al. 2002; Chieffi & Limongi 2004; Woosley & Heger 2007; Pignatari et al. 2016; Limongi & Chieffi 2018) but has been less well studied for binary progenitors (Braun & Langer 1995b; Brinkman et al. 2019, 2021; see, however, Izzard 2004; Izzard et al. 2006) The primary uncertainty in the nucleosynthetic yields of CC supernovae is whether the

star explodes and forms a neutron star (NS), ejecting its envelope, or collapses into a black hole (BH), where the envelope accretes onto the BH. The boundary between these fates is uncertain (Heger et al. 2003; Ertl et al. 2016; Boccioli et al. 2022), with binary interactions adding additional complexity (Timmes et al. 1996; Brown et al. 2001; Podsiadlowski et al. 2004).

Chemical enrichment of galaxies provides a direct test of both the formation of stars and their evolution (Tinsley 1980; Pagel & Tautvaisiene 1997), though these have also still mostly relied upon single-star models (Nomoto et al. 2013; Kobayashi et al. 2020; see however De Donder & Vanbeveren 2004). Wide-field Spectroscopic surveys (such as APOGEE Majewski et al. 2017), combined with Gaia (Gaia Collaboration et al. 2021, 2022) are revealing the chemical composition and evolution of the Milky Way (Perryman et al. 2001; Lian et al. 2022).

Massive stars are not the only source of chemical enrichment in the Universe (Burbidge et al. 1957). Other sources include the Big Bang (Peebles 1966; Wagoner et al. 1967), asymptotic giant branch (AGB) stars (van den Hoek & Groenewegen 1997; Herwig 2005; Karakas 2010), type Ia SNe (Woosley & Weaver 1994; Nomoto et al. 1997; Iwamoto et al. 1999; Eitner et al. 2022), and double neutron star mergers (Freiburghaus et al. 1999; Arnould et al. 2007; Kasen et al. 2017; Pian et al. 2017; Tanvir et al. 2017). Each source leaves a different chemical fingerprint on the composition of the Universe. Each source also contributes different elements and at different times (Carigi et al. 2005; Cescutti et al. 2009). For instance, massive stars evolve rapidly and can enrich the Universe in a few million years after star formation occurs (Franchini et al. 2020). While AGB (Nissen et al. 2014), SN Ia (Leung & Nomoto 2020), and double neutron star mergers (Dominik et al. 2012, 2013) take much longer to enrich the Universe, due to the slower evolution of their progenitor stars and/or long gravitational-wave inspiral times before merger.

In Section 2 we discuss our evolution of single and binary stars, and the properties of our explosion models. In Section 3 we discuss the total chemical yields from different mass-loss processes, while Section 4 breaks down the pre-supernovae yields and section 5 discuss the post-supernovae yields. Section 6 discusses several caveats with our results. Finally we discuss and conclude our results in Sections 7 and 8.

2. METHOD

This work builds upon the work in Farmer et al. (2021), which explored the chemical yields of ^{12}C , to extend the discussion to a larger set of isotopes (162) up to ^{64}Zn . We evolve a grid of single stars and binary-

stripped stars using the MESA stellar evolution code (version 12115, Paxton et al. 2011, 2013, 2015, 2018, 2019; Jermyn et al. 2022). These stars are evolved from the zero-age main sequence to core collapse and then through their supernovae until shock breakout. Our single stars and the primary (initially most massive star) in the binary have initial masses between $M_{\text{init}} = 11 - 45 M_{\odot}$. For binary stars we set the initial period to be between 38–300 days and we use a mass ratio of $M_2/M_1 = 0.8$ to set each secondary star’s mass. The orbital period chosen for each system ensures that all the binary stars undergo case B mass transfer (Paczynski 1967; van den Heuvel 1969). We follow the mass transfer from the primary star in the binary onto the companion assuming fully conservative mass transfer during Roche-lobe overflow (RLOF).

All models are computed with an initial solar metallicity of $Z=0.0142$ and are non-rotating. The single stars and binary stars are evolved with an initial $Y=0.2684$ ($Y = 2Z + 0.24$, Pols et al. 1995a; Tout et al. 1996). All stars are set to have the same initial composition profile, and is based on the solar composition of Grevesse & Sauval (1998). Additional physics options are specified in Appendix A. Four models did not reach core collapse and are excluded from this analysis, these are the binary-stripped star models with initial masses of 24, 25, 28, and $29 M_{\odot}$.

Inlists with all input parameters, data tables, and auxiliary data are made available online at <https://doi.org/10.5281/zenodo.5929870>. A sample of the data available is shown in Appendix B. While we have selected theoretically and observationally motivated assumptions for our input physics, we have not performed a systematic calibration of our models as we are interested in the *relative* differences between the chemical yields of binary-stripped and single stars.

To simplify our models we evolve the primary star in a binary system with a point-mass companion until the end of core helium burning. At this point we remove the companion and continue the evolution of the binary until core collapse, assuming these systems will not interact again (Laplace et al. 2020). Assuming that the Roche-lobe radius does not decrease after core helium burning and comparing that with the maximum radial extent of our binary stars post core helium burning, we find that this is a good approximation except for the $M_{\text{init}} = 22$ and $27 M_{\odot}$ models which would exceed their Roche-lobe radii (measured at core helium depletion), and the $M_{\text{init}} = 23 M_{\odot}$ which reaches 80% of its Roche-lobe radius (measured at core helium depletion). For all other binary-stripped stars the maximum radius is $< 10\%$ of their Roche-lobe radii (measured at core

helium depletion). Whether these stars would interact again, depends on detailed modelling of the accretor, as any mass it loses via winds would widen the orbit preventing further mass transfer phases.

Our choice of physics and modelling assumptions were described in Farmer et al. (2021) and builds upon the work presented in Laplace et al. (2020, 2021). We update our choice of convective overshoot in “metal” burning regions (regions burning elements heavier than helium) to an exponential profile (instead of a step overshoot profile). For that overshooting we assume a value of $f = 0.03$ and $f_0 = 0.001$ above the metal burning regions and $f = 0.003$ and $f_0 = 0.0001$ below the metal burning regions (Jones et al. 2017), where f is the extent of the overshoot region in pressure scale heights and f_0 is the point inside the convection zone where the strength of convective overshoot begins exponentially decaying (in pressure scale heights). For the other overshoot regions we assume a step overshoot profile with $f = 0.385$ and $f_0 = 0.05$ (Brott et al. 2011). We use the wind prescriptions of de Jager et al. (1988); Nugis & Lamers (2000); Vink et al. (2001) (“Dutch”), with a wind efficiency of 1.0. We include semiconvective mixing with a $\alpha_{\text{semi}} = 1.0$ and do not include thermohaline mixing (Farmer et al. 2016). We also include MLT++ to improve the numerical stability of the hydrogen envelopes (Paxton et al. 2013).

The larger nuclear network we adopt, compared to Farmer et al. (2021), is not only necessary for our yield predictions but is also important to capture important physics associated with the evolution up to core collapse (Farmer et al. 2016). We use a 162 isotope nuclear network which contains MESA’s `mesa_161.net`¹ network plus ⁴⁷Ca, for all evolutionary stages including the supernova phase. This network was chosen as a balance between larger networks (to capture more physics) and being computationally feasible. The addition of ⁴⁷Ca was so that we could cover all isotopes that were found to be of interest for next generation gamma-ray observatories (Timmes et al. 2019; Andrews et al. 2020).

We define the helium core mass of the star as where the helium mass fraction, $X_{\text{He}} > 0.1$ and the hydrogen mass fraction (at the same mass coordinate) is $X_{\text{H}} < 0.01$. Finally, we define core collapse to occur when the inner regions of the star infall at 300km s^{-1} .

¹ This network misses several stable isotopes, namely ⁶⁵Cu, ^{66–68}Zn, and ⁷⁰Zn.

We define the yield of an isotope as (Karakas & Lugaro 2016):

$$\text{Yield} = \sum_{\text{T}} \Delta M_{\text{T}} \times (X_{\text{j}} - X_{\text{j,init}}) \quad (1)$$

where ΔM_{T} is the mass loss in $M_{\odot} \text{yr}^{-1}$ over the time T in years, X_{j} is the mass fraction of species j , and $X_{\text{j,init}}$ is the initial mass fraction of that species.

At the point of core collapse we define the core compactness parameter as (O’Connor & Ott 2011):

$$\xi_M = \frac{M/M_{\odot}}{R(M = 2.5 M_{\odot})/1000\text{km}} \quad (2)$$

where M is the enclosed mass (taken as $2.5 M_{\odot}$) and R is the radius at this mass coordinate in km. As there are multiple criteria possible for determining the explosibility of a model, we also use the criteria of Ertl et al. (2016) following the `w18.0` fit, defining models to explode as those with:

$$\mu_4 < 0.283M_4\mu_4 + 0.0430 \quad (3)$$

where M_4 is the mass coordinate (in solar masses) where the entropy per nucleon $S = 4$, and μ_4 is the mass gradient at this mass coordinate, defined as:

$$\mu_4 = \left. \frac{\Delta m/M_{\odot}}{\Delta r/1000\text{km}} \right|_{S=4} \quad (4)$$

where we adopt a $\Delta M = 0.3 M_{\odot}$ and Δr is the change in radius at $S=4$ over ΔM .

2.1. Core-collapse supernovae

Our explosion models follow those of Farmer et al. (2021). We first excise the inner region of each star’s core, by placing the inner boundary of our model at the point where the entropy per baryon $S = 4$ (Brown & Woosley 2013). We then use a thermal bomb, placed at the inner boundary of the model to inject energy into the star (Aufderheide et al. 1991; Sawada & Maeda 2019). We do not allow the model to collapse further inwards after the excising the core, which can alter the final nucleosynthetic signal (Imasheva et al. 2023). In our default model, energy is then injected over the inner $0.01 M_{\odot}$ and over 0.0045 seconds. We inject sufficient energy to bring the total energy of the star (the sum of the kinetic plus thermal energy minus the gravitational binding energy) to 10^{51}erg/s . While there is some evidence for choosing different explosion parameters between stripped envelope supernovae and non-stripped supernovae (Saito et al. 2022), we chose to use a constant set of parameters to minimise the parameter space explored. In Section 5.4 we show the uncertainty

introduced into the final yields due to differences in the explosion parameters.

The energy we inject into the star is sufficient to drive a hydrodynamic shock that travels outwards from the center of our model to the surface. We stop our models once the shock reaches $0.1 M_{\odot}$ below the surface. In [Farmer et al. \(2021\)](#) we found that the final total energy of a star would be 5–20% higher than what was injected into the star during the explosion. This was due to the change in the nuclear networks (between the end of the stellar evolution and the start of the supernovae) introducing new isotopes that were not in nuclear statistical equilibrium (NSE)². In this work, as we have used the same nuclear network for the entire stars evolution, the core maintains NSE between the stellar evolution and core collapse phases. The difference in final total energy of the star compared to the total energy after the energy injection phase is now $< 1\%$.

2.2. Stable isotopes

Many of the isotopes in our 162 isotope nuclear network are short-lived radioactive isotopes and thus would not be expected to contribute to the Galactic yields. Therefore, we also compute the set of stable isotopes converting each radioactive isotope into its single most probable decay product (Timmes, F., priv. com.). This is effectively assuming that we observe the isotopes on a timescale much longer than their half-lives, and that each isotope has only one decay channel³.

3. TOTAL EJECTA

We define the fraction of each isotope F_i which is ejected by either single or binary stars in different mass-loss processes as:

$$F_i = \frac{\int_{11}^{45} (E_{pre,i} + f_{SN} E_{post,i}) m^{\alpha} dm}{\sum_{b,s} \int_{11}^{45} (E_{pre,i} + f_{SN} E_{post,i}) m^{\alpha} dm} \quad (5)$$

where $E_{pre,i}$ ($E_{post,i}$) is the ejected mass of isotope i , from the pre-SN mass loss (post-SN mass loss) from either the binary-stripped (b) or single stars (s). This is then integrated over the mass range m (in solar masses) and weighted by the initial mass function (IMF), with an assumed power law $\alpha = -2.3$ ([Salpeter 1954](#); [Schneider et al. 2018](#)). The factor f_{SN} is a term that is set to

control whether or not we include the contribution from a star’s post-SN mass loss, depending on whether the envelope is ejected ($f_{SN} = 1$) or not ($f_{SN} = 0$). This is then normalized by summing over the IMF-weighted contributions from all mass loss processes for both single and binary stars. For the binary-stripped models which did not evolve to CC, we interpolate their wind yields over the failed models, and assume that they would not successfully eject their envelopes during core collapse.

Figure 1 shows the results of Equation 5, which breaks down whether each element was ejected during wind mass loss or RLOF assuming the secondary star was able to later eject the material unprocessed (pre-SN), or in the supernova ejecta (SN). For the supernovae ejecta we assume the explosion model given by equation 3 of [Ertl et al. \(2016\)](#) (See section 5.1) to set the filter term f_{SN} . Panel (a) shows all elements while panel (b) shows the result of decaying all unstable isotopes to their most probable stable product. This assumes that the ratio of single stars to binary-stripped stars is approximately equal ([Sana et al. 2012](#)).

We draw several broad conclusions from Figure 1. Firstly, massive binaries in general produce larger fractions of most elements compared to massive single stars (50–60% of the total yield). Most light elements ($Z < 8$), lighter than oxygen, are ejected during wind mass loss (or RLOF), while newly-synthesized heavier elements unsurprisingly require a supernova to be ejected. Binary-stripped stars are also able to eject a significant fraction of unstable isotopes with $20 < Z < 27$ (calcium to cobalt) in their pre-SN mass loss (See section 4.1). Stable elements in the $20 < Z < 27$ (calcium to cobalt) range, in pre-SN mass loss, are produced in their helium cores via neutron captures. Thus stripped binaries are able to eject more of those isotopes than single stars, as they expose their helium cores earlier, allowing for a greater total amount of mass to be ejected from their helium cores. The same effect is responsible for the increased ^{12}C production in binary-stripped stellar winds ([Farmer et al. 2021](#)).

The large spike at $Z=9$ (fluorine) for the binary SN ejecta in Figure 1(a) is due to the production of the short lived isotope ^{18}F which decays to ^{18}O . The source of stable fluorine is still uncertain ([Renda et al. 2004](#); [Lugaro et al. 2008](#); [Franco et al. 2021](#)), but Figure 1(b) indicates that massive binaries can make more overall than massive single stars. Though the final yield will depend on neutrino spallation of ^{20}Ne in the supernovae shock, which we do not follow ([Woosley & Haxton 1988](#); [Woosley et al. 2002](#)). This increased production of fluorine is due to two factors, firstly the wind yields are higher in binary-stripped stars, due to positive yields

² MESA does not assume NSE, instead it uses the same nuclear network integration that is used at lower temperatures ([Paxton et al. 2015](#))

³ This assumption is reasonable for most isotopes in our network except for ^{36}Cl , ^{46}Sc , ^{54}Mn , ^{58}Co , ^{64}Cu where additional decay channels can play a role.

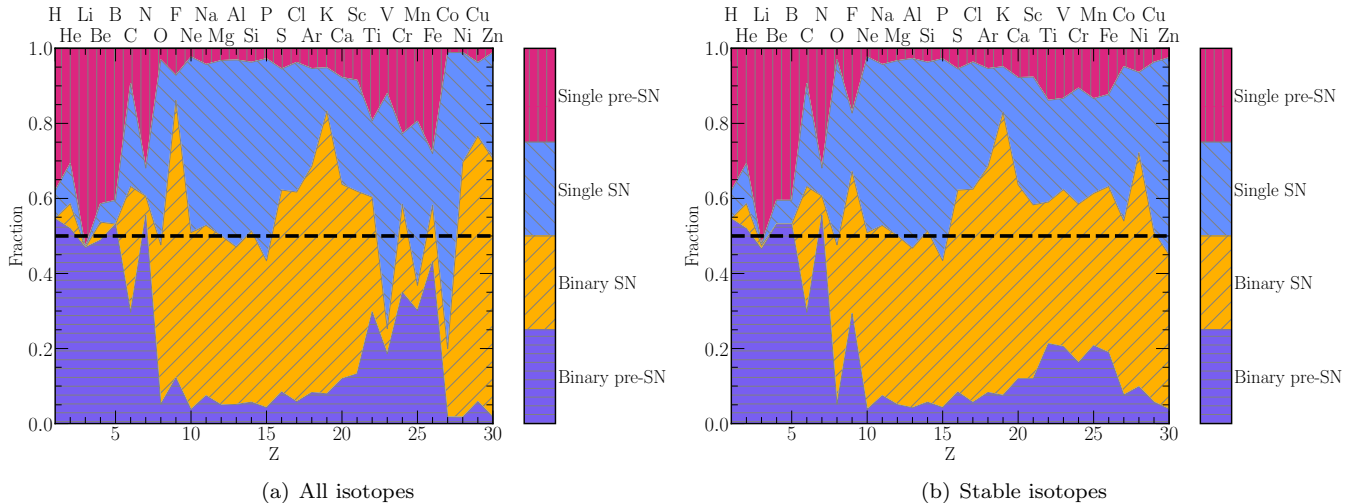


Figure 1. Fraction of the IMF-weighted ejecta (not yields) per element as a function of the different formation channels. Pre-SN denotes all pre-supernova mass loss (wind mass loss and RLOF), while SN denotes the ejecta from successful SN (using the Ertl et al. (2016) criterion). Panel (a) shows the contribution from all isotopes, while panel (b) shows only the stable isotopes after decaying all radioactive isotopes to their most likely decay product. Vertical (horizontal) hatching shows the single (binary) star pre-supernovae mass loss while reverse (forward) diagonal hatching shows the single (binary) supernovae mass loss.

only occurring in stars that expose their C/O cores during core helium burning (Meynet & Arnould 2000). Secondly the supernovae yields peak for the lowest-mass binary-stripped models, which are then favoured by the IMF.

At core collapse ^{19}F is produced via the chain $^{14}\text{N}(\alpha, \gamma)^{18}\text{F}(\beta^+)^{18}\text{O}(p, \alpha)^{15}\text{N}(\alpha, \gamma)^{19}\text{F}$ (Goriely et al. 1990; Limongi & Chieffi 2018), at the base of the helium shell. In the binary-stripped models this shell is slightly cooler ($\log(T/K) \approx 8.3$) than in single stars ($\log(T/K) \approx 8.5$) at core collapse. This leads to an increased destruction of ^{18}O in the single star models, which limits the production of ^{19}F .

Figure 1 shows that potassium is the element most affected by binary physics, with most of its contribution coming from the SN ejecta of binary-stripped stars. Potassium abundances have been challenging to fit in previous models of chemical enrichment (Kobayashi et al. 2020), which suggests the binary-stripped stars may be the key to its production. This peak is predominantly from ^{39}K produced by our low mass binary-stripped stars during their pre-supernovae evolution. The potassium is produced just outside what will become the compact object, inside the silicon rich-layers. The amount of ^{39}K produced is correlated with the size of this layer and thus may depend sensitively on the uncertain properties of convection during Si/Fe burning.

Around $Z \approx 25$ (manganese), single stars produce more odd- Z nuclei in their supernovae while even- Z nuclei are produced equally by single and binary stars.

This is due to vanadium being produced in the single stars that are still red super giants (RSG) at core collapse (these have a low initial masses and are thus highly weighted by the IMF). This vanadium then forms a seed for alpha captures that then produce manganese and cobalt. Stars that have lost their H-envelopes (either stars stripped in binaries or high-mass single stars) produce much less vanadium during core collapse, thus there are less seed nuclei present for this odd-even pattern. This pattern disappears however when considering only the stable decay products, therefore a detectable signal will depend heavily on the timing of the observations relative to the explosion.

In the online Zenodo material we provide the yields for all isotopes from all mass-loss processes, as well as diagnostic information about the stellar models. See Appendix B for an example of the data provided.

4. PRE-SUPERNOVA EVOLUTION

During the pre-supernova evolution of our models the chemical yield is affected by both the wind mass loss and the mass lost during RLOF (for binaries). This difference in mass-loss processes has two effects on the yields, firstly it changes the total mass loss and the timing when that mass is lost, secondly the mass loss has an effect on the core structure of the star leading to changes in its composition and core mass (Kippenhahn & Weigert 1967; Habets 1986; Laplace et al. 2021). In general the greater the fraction of the star’s mass that is lost, and the earlier that it is lost in the star’s life, the lower the final core mass becomes.

4.1. Composition of stellar winds

Figure 1 shows that the pre-supernovae mass loss contributes almost the entirety of the chemical yields for low-mass elements. For higher-mass elements, massive binary-stripped stars are able to eject $\approx 20\%$ of their total ejecta in iron-group elements, while for massive single stars this is closer to $\approx 10\%$. This occurs due to the increased mass loss in the binary-stripped stars exposing the He-core during core helium burning. This material is enriched in neutron capture isotopes (see also the much larger contribution of the binary pre-SN mass loss in Figure 1a). These neutrons come primarily from $^{22}\text{Ne}(\alpha, n)^{25}\text{Mg}$ (Prantzos et al. 1987). See Appendix C for a discussion of the sensitivity of the isotopic yields due to the wind-scaling factor, and hence total wind mass loss.

We can divide the yields into 3 broad categories: 1) those that change approximately linearly with mass lost (e.g. ^1H , ^4He) either positively or negatively; 2) those that are small or negative until the star exposes its helium core (e.g. ^{12}C or ^{19}F) before increasing; 3) those that fall into neither of those categories, which we discuss below.

4.1.1. ^{17}O

For massive single stars ^{17}O has positive yields only for stars with $M_{\text{init}} < 31 M_{\odot}$, with the yield increasing as the initial mass decreases. The peak formation is at $M_{\text{init}} = 18 M_{\odot}$ before the yield then decreases at even lower masses. For massive binary stars the yields are positive for masses below $M_{\text{init}} \lesssim 25 M_{\odot}$, with no turnover in the yields. The stripped binaries have larger yields than single stars below $M_{\text{init}} < 16 M_{\odot}$.

4.1.2. ^{24}Mg

Both our stripped binaries and single stars show positive yields for ^{24}Mg . However, for single stars the yields peak at $M_{\text{init}} = 36 M_{\odot}$ (when the star exposes its helium core), before decreasing at higher masses. In contrast, for the binaries the yield always increases as the initial mass increases.

4.1.3. ^{51}V

We find that ^{51}V is the only isotope in our nuclear network that has a positive wind yield from binary-stripped massive stars while having a negative wind yield from single stars. While this would make wind mass loss from stripped-binaries an candidate source of ^{51}V we find that the total yield of ^{51}V is dominated by the core-collapse yields from single stars. Electron captures onto vanadium can play a key role in setting the final electron fraction of the core before collapse (Aufderheide et al. 1994; Heger et al. 2001).

4.2. Composition of mass lost during RLOF

Farmer et al. (2021) showed that the mass transferred during Case B RLOF stripping is not enriched in ^{12}C compared to the initial abundances, however the structural changes caused by the extra mass loss would affect the star's evolution, and thus the final ^{12}C yield. This was due to the fact that ^{12}C was primarily produced during core helium burning which occurred *after* mass transfer finished.

However, there are also a number of isotopes that are produced in hydrogen envelopes and thus can be ejected *during* the mass transfer process. These are generally light elements that are either produced in the low temperature environment of the hydrogen envelope or are able to be mixed out of the hydrogen core/shell into the envelope and then ejected.

Figure 1(b) shows similar total ejecta from single and binary-stripped massive stars. However, the net contribution to the Universe will be reduced in the binary-stripped stars as compared to single stars, as their contribution to the composition of the Universe will depend sensitively on how conservative mass transfer is and how the secondary reprocesses and re-ejects any accreted material. We assume for the calculation of the RLOF phase that all the material we eject from the donor accretes onto the accretor (fully conservative). However, we track these isotopes separately and can infer what the composition might be if some fraction of this accreted material is ejected during RLOF or is re-ejected later by the accretor without further nuclear processing as a wind. We will note when we include the contribution from RLOF (or not). Overall, for elements Phosphorus ($Z=15$) and heavier, the absolute yields from RLOF are $< 1\%$ of the absolute wind yields. While for lighter elements the absolute RLOF yields can be comparable to the absolute wind yields.

Figure 2 shows the relative contribution to the IMF-weighted yield from pre-SN mass loss, due to RLOF and stellar winds. Red regions signify that the isotope is predominately ejected in stellar winds, while blue signifies that the isotope is predominately ejected during RLOF. The blue regions show that ^{13}C , ^{14}N , and ^{21}Ne are primarily ejected during RLOF (we ignore ^7Be from this discussion, see section 6.2).

As the hydrogen-burning core recedes it will leave behind CNO processed material, allowing the envelope to be enriched in ^{14}N which is then ejected during RLOF. The NeNa-cycle is able to convert hydrogen to helium (similar to the CNO cycle) via neon, sodium, and magnesium. Above temperatures of $T > 3.5 \times 10^7\text{K}$ ^{21}Ne is destroyed via $^{21}\text{Ne}(p, \gamma)^{22}\text{Na}(\beta^+)^{22}\text{Ne}$, while below this temperature ^{21}Ne is produced via

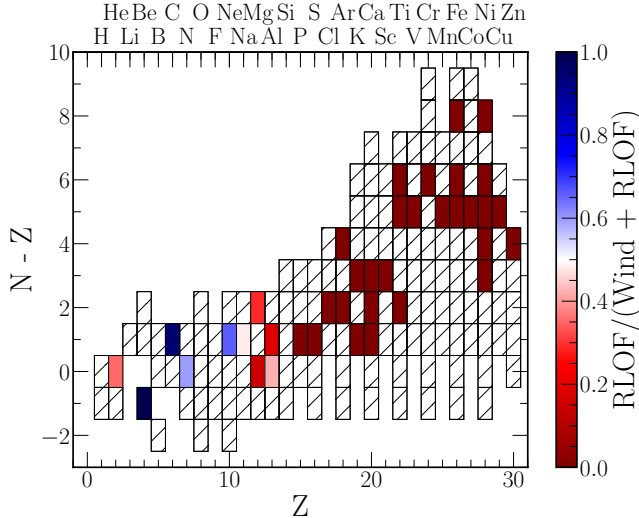


Figure 2. The IMF weighted relative yield fraction of ejected isotopes from RLOF compared to wind mass loss in binary systems. The x-axis is the proton number, Z , while the y axis is the number of neutrons (N) minus the number of protons (Z). Hatched squares indicate that one or both ejection processes (RLOF or winds) have negative yields or the yields from either RLOF or wind mass loss are below $10^{-15} M_{\odot}$.

^{20}Ne (p, γ) ^{21}Na (β^+) ^{21}Ne (Wiescher & Langanke 1986; José et al. 1999). The amount of ^{21}Ne is maximised when there is H burning in the temperature range $3 \leq T/10^7\text{K} \leq 3.5$ (Arnould et al. 1999). Thus significant amounts of ^{21}Ne can only be ejected if the material is burnt in the H-shell and mixed outwards before the H-shell can further process the material.

^{13}C can provide a significant fraction of the neutron flux at stellar densities and temperatures, via the reaction $^{13}\text{C}(\alpha, n)^{16}\text{O}$ (Busso et al. 1999), thus its production (and destruction) plays a key role in the s-process (Gallino et al. 1998). The ratio of $^{12}\text{C}/^{13}\text{C}$ has also been used as a probe of galactic chemical evolution (Milam et al. 2005).

Table 1 shows the IMF weighted $^{12}\text{C}/^{13}\text{C}$ ratio from the different mass loss processes. The totals show the $^{12}\text{C}/^{13}\text{C}$ ratio depending on whether the mass donated by the primary is ejected from the system (with RLOF) or is assumed to be accreted onto the accretor and mixed inwards (without RLOF), thus not being ejected into the Universe. This assumes the accretor does not re-eject the material at a later time. Table 1 therefore indicates that the contribution to the Galactic $^{12}\text{C}/^{13}\text{C}$ from massive stars will depend sensitivity on how conservative mass transfer is, thus how much mass is accreted, and whether the accretor re-ejects the material or it is mixed into the core. Thus the $^{12}\text{C}/^{13}\text{C}$ ratio in

Table 1. The ratio of the IMF integrated $^{12}\text{C}/^{13}\text{C}$ ejected during different mass loss processes.

	Single	Binary
Winds	50	802
RLOF	-	17
pre-SN total	50	123
post-SN total	360	321
Total including RLOF	154	193
Total not including RLOF	154	446

regions where the dominant enrichment is from massive stars could potentially be used as a tracer of how conservative mass transfer is, as the ejection of ^{13}C occurs primarily during the mass transfer process, while ^{12}C is primarily ejected from WR wind mass loss.

The Solar system has $^{12}\text{C}/^{13}\text{C} \approx 90$ (Romano et al. 2019; Botelho et al. 2020), which is lower than the values in Table 1, thus the primary producer of ^{13}C is likely lower-mass stars, for instance AGB and TP-AGB stars which can have $^{12}\text{C}/^{13}\text{C}$ values between ~ 10 –180 depending on the initial mass (Karakas & Lugaro 2016).

4.3. Core composition

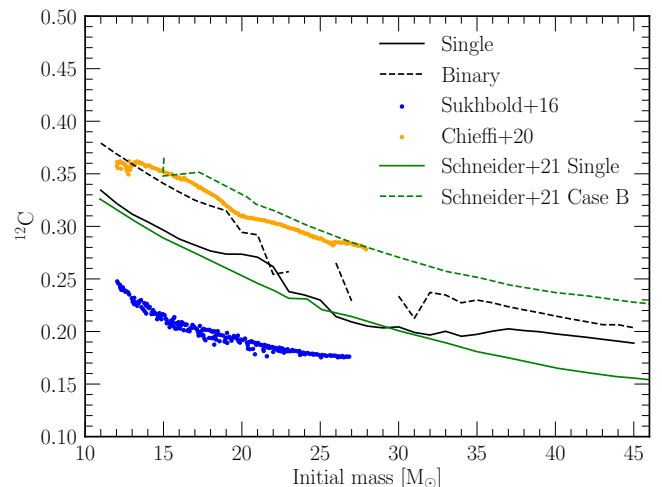


Figure 3. Comparison of ^{12}C mass fractions at the end of core helium burning. Black solid line: Single stars, Black dashed line: Binary-stripped stars, Blue: Sukhbold et al. (2016), Orange: Chieffi & Limongi (2020), Green solid line: Single star models from Schneider et al. (2021), Green dashed line: Case B binary models from Schneider et al. (2021).

The final fate of a star depends on many quantities, however the core mass and the central ^{12}C fraction at the end of core helium burning are two of the most important (Chieffi & Limongi 2020; Patton & Sukhbold 2020). Figure 3 shows a comparison of the core C fraction at the end of core helium depletion for various solar metallicity models. In general we can see that as the initial mass increases, the core ^{12}C fraction decreases. It is set by the combination of the 3α rate and the $^{12}\text{C}(\alpha, \gamma)^{16}\text{O}$ reaction (Sukhbold & Adams 2020). For our single star models, the ^{12}C fraction agrees well with Schneider et al. (2021), which is unsurprising as Schneider et al. (2021) also used MESA with similar physics choices, although there is a divergence at high initial mass, which may be due to our different choices of chemical mixing. Schneider et al. (2021) also uses a similar wind prescription as this work, but with a different dependence on the metallicity.

Our binary-stripped models also closely match the values of Schneider et al. (2021) case-B binaries, with differences likely due to the different method of removing the envelope, as Schneider et al. (2021) takes the material off with an ad-hoc prescription, while we follow the binary mass transfer. Our models show a variability in the ^{12}C trend, not seen in Schneider et al. (2021), in the 20–30 M_{\odot} mass range. This is where both the MLT++ approximation is important and the envelope is not significantly removed by winds before mass transfer begins. Thus the envelopes properties depend sensitively on the ad-hoc MLT++ prescription, which propagates as an uncertainty in how wind mass loss occurs, and how efficient RLOF is at removing the envelope. How mass is lost from a star has been shown to significantly impact the internal structure of massive stars (Renzo et al. 2017).

Our binary-stripped models also agree well with the Chieffi & Limongi (2020) single star models, for $M_{\text{init}} < 20 M_{\odot}$. Both Chieffi & Limongi (2020) and this work use NACRE (Angulo et al. 1999) for the 3α rate. For the $^{12}\text{C}(\alpha, \gamma)^{16}\text{O}$ rate Chieffi & Limongi (2020) uses Kunz et al. (2002) while we use Angulo et al. (1999) rate. Therefore differences likely stem from different choices in the nuclear physics. Thus binary stripping has a similar effect on the core abundance as variations in the $^{12}\text{C}(\alpha, \gamma)^{16}\text{O}$ reaction rate.

As shown extensively in Laplace et al. (2021) the effect of the extra mass loss due to RLOF causes structural changes to the cores of massive stars. These changes cause the cores to become smaller (in mass) and to have extended chemical gradients. This leads to differences in the intensity and timing of nuclear shell burning episodes, which compounds the differences between

single and binary-stripped stars. While Farmer et al. (2021) has shown how the binary interactions affect the final ^{12}C yield.

Details of key stellar properties can be found in Appendix D and in Tables 3 and 4. These include the final total and core mass, total mass lost to different mass loss processes, and final masses of H, He, and C.

5. SUPERNOVAE

The nucleosynthetic yields from core-collapse supernovae are the result of (i) whether or not the star can successfully explode and produce ejecta and (ii) the pre-collapse structure and composition.

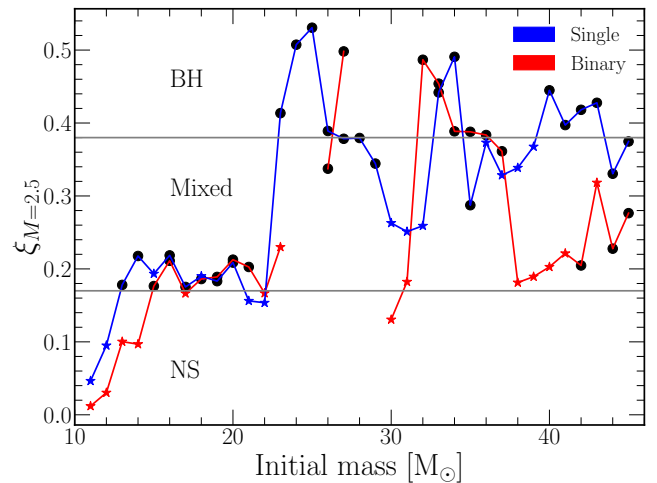


Figure 4. The compactness parameter as a function of the initial stellar mass for massive single stars (blue) and binary stars (red). The grey lines mark $\xi_{M=2.5} = 0.16$ and $\xi_{M=2.5} = 0.36$ (with dm averaged over $0.3 M_{\odot}$) as the approximate boundaries between all models undergoing a successful explosion ($\xi_{M=2.5} \leq 0.16$), no model undergoing a successful explosion ($\xi_{M=2.5} \geq 0.36$), and an intermediate mixed state. Star symbols mark models that would successfully explode under the two-component fit of Ertl et al. (2016) calibrated against the model w18.0, while black circles denote models that would not be expected to produce successful explosions (and thus ejecta).

5.1. Explodability

We first determine whether a star will successfully explode and eject its envelope, or not. Figure 4 shows two measures of a star’s explodability: its compactness (O’Connor & Ott 2011) (y-axis) and the two component fit of Ertl et al. (2016) (symbols), as a function of the initial mass. As shown in many other works (e.g. Sukhbold et al. 2016; Farmer et al. 2016; Renzo et al. 2017; Sukhbold & Adams 2020; Patton & Sukhbold 2020), the evolution to core collapse and the star’s final

structure is sensitive to the choice of physics, treatment of chemical mixing boundaries (Chieffi & Limongi 2020), and numerical choices (Farmer et al. 2016) made by the software instrument used. In Figure 4 we define three regions based on the two component fit of Ertl et al. (2016)⁴. One region contains models that only make NSs ($\xi_{M=2.5} \leq 0.16$), another contains those that only make BHs ($\xi_{M=2.5} \geq 0.36$), and there is an intermediate region in which we consider the outcomes to be less certain. The boundaries of these regions are almost the same as the boundaries found by Ugliano et al. (2012) ($\xi_{M=2.5} \leq 0.15$ for NS and $\xi_{M=2.5} \geq 0.35$ for BH). But the presence of the mixed region shows why the compactness, on its own, is not a good measure for determining the explosion outcome.

In Figure 4 we can find several regions that are expected to undergo successful explosions, with only slight movement of the boundaries between single and binary stars. Between $11 < M_{\text{init}}/M_{\odot} < 21$ and $31 < M_{\text{init}}/M_{\odot} < 36$ stars end their lives with similar compactness parameters (and with similar explosion success metrics). In contrast, between $21 < M_{\text{init}}/M_{\odot} < 31$ (though there are a number of missing models here) and $M_{\text{init}} > 38 M_{\odot}$ the final states of the stars are very different between single and binary-stripped stars, leading to differences both in the explodability and their final nucleosynthetic yields.

The structure seen in Figure 4 is related to the transition in how different fuels ignite in the core (Sukhbold & Woosley 2014; Laplace et al. 2021). The peak at $M_{\text{init}} \approx 25 M_{\odot}$ is when carbon changes from central to off-center burning while the peak at $M_{\text{init}} \approx 34 M_{\odot}$ is coincident with neon going from central to off-center burning (Schneider et al. 2021). The shift in the location of the peaks between binary-stripped and single stars is due to the binary-stripped stars having smaller core masses, due to the core receding when RLOF removed the envelope (Farmer et al. 2021).

We include the fallback prescription of Goldberg et al. (2019). Here zones near the inner boundary are removed that have a total energy, when integrated from the core to the zone, that is negative. This is done by moving the inner boundary of the model to the point where the material has a positive total energy, and thus is unbound from the core. This is repeated at each time step. See Appendix A of Goldberg et al. (2019) and Paxton et al. (2015) for the full details of this fallback treatment. For the models presented here and with our default ex-

plosion parameters, the amount of fallback is negligible ($\Delta M \lesssim 10^{-3} M_{\odot}$) even in cases that do not formally explode via the Ertl et al. (2016) criterion. As the amount of fallback is negligible in these models, for the choices of explosion physics used here, we simplify our modelling by using an explodability criterion. This lack of fallback is driven by our choice of a fixed 10^{51} erg/s explosion, lower energy explosions can have larger fallback masses with the prescription as implemented in MESA (Goldberg et al. 2019).

Schneider et al. (2021) found that for case B binaries (where they artificially remove the envelope), NS production occurs for $M_{\text{init}} \leq 31.5 M_{\odot}$ and $M_{\text{init}} > 34.0 M_{\odot}$, while for single stars the range is between $M_{\text{init}} \leq 21.5 M_{\odot}$ and $23.5 \leq M_{\text{init}}/M_{\odot} \leq 34.0$. These boundaries can shift if fallback accretion is taken into account (Timmeres et al. 1996). We find a somewhat more complex boundary between NS and BH formation for $M_{\text{init}} \leq 22 M_{\odot}$ and $M_{\text{init}} > 36 M_{\odot}$. Differences between the boundaries found by Schneider et al. (2021) and those in this work are likely due to differences in the physical assumptions, such as the choice of convective boundary mixing, timing of mass loss, and the choice of nuclear network. These have been shown to lead to large changes in the final structure (Farmer et al. 2016; Renzo et al. 2017; Farmer et al. 2021).

5.2. SN yields

Figure 5 shows a comparison between our $13 M_{\odot}$ single⁵ and binary-stripped stars with yields available in the literature⁶. Panel (a) shows the total elemental yields (as a sum of the stable isotopes), while Panel (b) shows the ratio of the elemental yield for our single star model as compared to the literature values. Our supernova models were exploded with our default explosion physics.

Overall, we over predict (as compared to the literature) elements in the $Z=10-21$ range by a factor of 5. For higher mass elements we have a good agreement with the Kepler based results (Sukhbold et al. 2016; Woosley 2018) while diverging to a factor 10 over prediction compared to the results of (Limongi & Chieffi 2018) which are based on the FRANEC code. Our large disagreement

⁴ See also Boccioli et al. (2022) for a potential new criterion for determining explodability

⁵ Formally our $13 M_{\odot}$ single star does not explode by any of the fits provided in Ertl et al. (2016), however given the limited range of initial masses in Limongi & Chieffi (2018) that overlap with our models, we chose this initial mass as the binary-stripped model comfortably forms a NS, while both the $15 M_{\odot}$ models are on the edge between NS and BH, the $20 M_{\odot}$ models both make BHs, and we have no model for a $25 M_{\odot}$ stripped-binary.

⁶ We made use of the VICE (Johnson & Weinberg 2020; Johnson et al. 2021; Griffith et al. 2021) software package to provide this information.

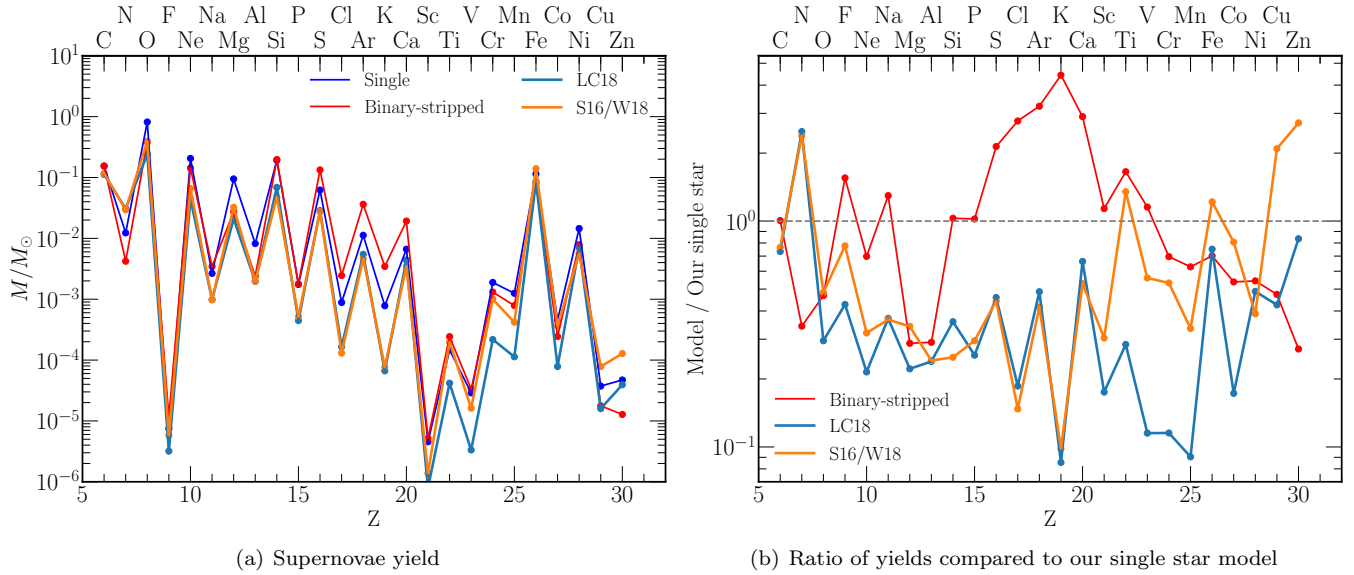


Figure 5. Panel (a): The stable isotopic yields from core collapse for a $13 M_{\odot}$ star from the literature; LC18 (Limongi & Chieffi 2018): light blue, S16/W18 (Sukhbold et al. 2016; Woosley 2018): orange) as compared to our $M_{\text{init}} = 13 M_{\odot}$ single (dark blue) and $M_{\text{init}} = 13 M_{\odot}$ binary-stripped star (red). Panel (b): The ratio of the core collapse stable yields from the literature and our $M_{\text{init}} = 13 M_{\odot}$ binary-stripped star compared to our $M_{\text{init}} = 13 M_{\odot}$ single star.

for Zinc is due to the fact that our nuclear network stops at Zinc, thus isotopes will pile up at the edge unable to produce heavier isotopes. Other differences are likely due to differences in the stellar micro-physics and physical assumptions. For instance, we showed in Farmer et al. (2021) that the, currently unconstrained, choice for the amount of overshoot during carbon burning can have a significant impact on the carbon yields, that would then propagate as an uncertainty on the product of carbon burning namely ^{20}Ne , ^{23}Na , and ^{24}Mg . This is due to a ^{12}C yield being sensitive to the size of the pocket of C that survives, between the top of the final carbon-burning shell and the helium shell (Farmer et al. 2021). This pocket, however, can be eroded by convective overshoot from the final convective carbon-burning shells.

Figure 5b also shows the comparison between a binary-stripped model and a single star model, for the same initial mass. Here we can see that the binary-stripped model produces more of the intermediate-mass elements ($15 < Z < 24$) by up to a factor ≈ 4 , while producing slightly less of the higher mass elements ($Z > 24$), as well as producing less magnesium and aluminum ($Z=12$ and $Z=13$).

5.3. Explosive nucleosynthesis

Figure 6 shows the relative change in the IMF-weighted material ejected in a SN between its pre-SN composition and its post-SN composition. Blue regions indicate isotopes that are produced in the SN while red regions indicate isotopes that are destroyed in the SN.

The color bar has been truncated, to better show the details, however the (blue) material produced can peak at $\approx 10^{15}$ times more (for isotopes in the bottom right corner), and the (red) material destroyed peaks at only $\approx 10^4$ times less.

We can see in Figure 6 that most of the region of change occurs for $Z > 20$ and $N - Z < 4$. These are generally the proton-rich isotopes, that have very low abundances outside of the mass cut pre-SN. Thus even a small production during the SN causes a large relative increase in the composition. There is also an increase in the more neutron rich isotopes, typically expected for r-process, in the top right of each panel in Figure 6. This includes the isotope ^{60}Fe which is of interest for gamma-ray observations (Mahoney et al. 1982; Leising & Share 1994).

Comparing Figures 6(a) to 6(b), we can see that both show this enhancement in proton-rich isotopes, though the single stars show a greater fraction of material coming from the pre-SN evolution for the most proton-rich isotopes of Ti, Cr, and Fe. For the more neutron-rich isotopes ($N - Z \approx 8$), the single stars show material coming more from the explosive nucleosynthesis during the SN than before. For neutron-rich isotopes of Al–Sc, binary-stripped stars are generally producing this material pre-SN (and outside what will become the compact object), while in single stars this occurs during the explosive nucleosynthesis in the SN.

We reconfirm our finding the ^{12}C is not affected by the supernova shock (Farmer et al. 2021). We find, with

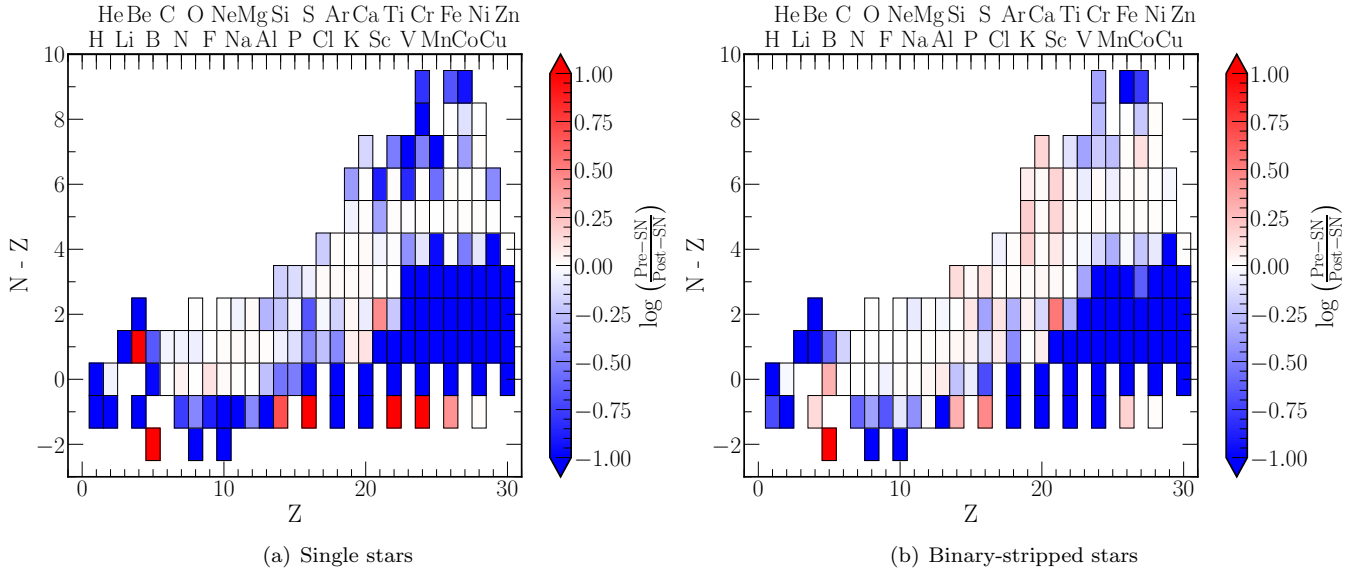


Figure 6. The logarithmic ratio of the IMF weighted pre-SN composition, outside of the mass cut, to the IMF weighted composition of the models near shock breakout. Blue indicates isotopes produced in the SN, while red indicate isotopes destroyed in the SN. We did not decay any isotopes to their stable versions. The colors are truncated to be between -1 and 1.

our larger number of isotopes, that ^{12}C is in fact the isotope least affected by the supernova explosion. This is due both to its location near the He-shell, thus little ^{12}C is lost to the formation of the compact object, and when the shock finally reaches the He-shell it has cooled sufficiently to be unable to drive additional ^{12}C burning.

5.4. SN uncertainties

Following the method of Farmer et al. (2021) we explore the sensitivity of our SN yields to the uncertain explosion physics. We took a $17M_{\odot}$ ⁷ single and binary-stripped star models and exploded each of them ≈ 100 times. For each sample we would randomly vary the following four parameters: the injection energy, mass cut, injection mass, and injection time. As an improvement over Farmer et al. (2021) we sample all four explosion parameters simultaneously as opposed to doing two grids, which sampled only two parameters at a time. We vary the injection energy between $0.5\text{--}5.0 \times 10^{51}\text{erg/s}$, the mass cut between $1.0\text{--}2.0M_{\odot}$, the injection mass $10^{-2}\text{--}5 \times 10^{-1}M_{\odot}$, and the injection time $10^{-3}\text{--}1.0\text{s}$. We assume a thermal bomb for our explosions, however a piston driven explosion may produce different yields for the same input energy (Young & Fryer 2007).

Figure 7 shows for which isotopes it is more important to understand the progenitor ($\log(\Delta\text{Explosion}/\Delta\text{Progenitor}) = -1.0$) and for which

isotopes it is more important to understand the explosion mechanism ($\log(\Delta\text{Explosion}/\Delta\text{Progenitor}) > -1.0$). Where $\Delta\text{Explosion}$ is the spread in the final ejecta composition for a $17M_{\odot}$ model where we vary the explosion physics, and $\Delta\text{Progenitor}$ is the spread in the final ejecta composition for fixed explosion physics but considering our entire range of initial masses. Both $\Delta\text{Explosion}$ and $\Delta\text{Progenitor}$ are defined separately for our single and binary-stripped stars.

Figure 7 also shows that there is a difference between single stars and binary-stripped stars in which isotopes are uncertain, and thus which types of supernovae could be used to constrain different isotopes if detectable either through spectroscopy or radioactive decay signatures. These differences occur due to the differences in the time needed for the shock to break out of the photosphere, in the less massive single stars (which still have a RSG envelope) shock breakout is approximately a day after the core collapses, while in our binary-stripped stars (and high-mass single stars that lose their H-envelopes) shock breakout occurs much less than a day after the core collapses. Thus stripped-envelope supernovae explode faster and have less time for short lived radioactive nuclei to decay before the shock breakout phase. This hints that stripped-envelope supernovae from binaries could be interesting locations to study radioactive decay products from explosive nucleosynthesis, with sufficiently early time observations and sufficient chemical mixing to bring them to the photosphere.

⁷ Our $17M_{\odot}$ single star model does not formally explode given the fits in Ertl et al. (2016), though it does have a similar compactness to the $17M_{\odot}$ binary-stripped model.

5.5. Gamma ray emitters

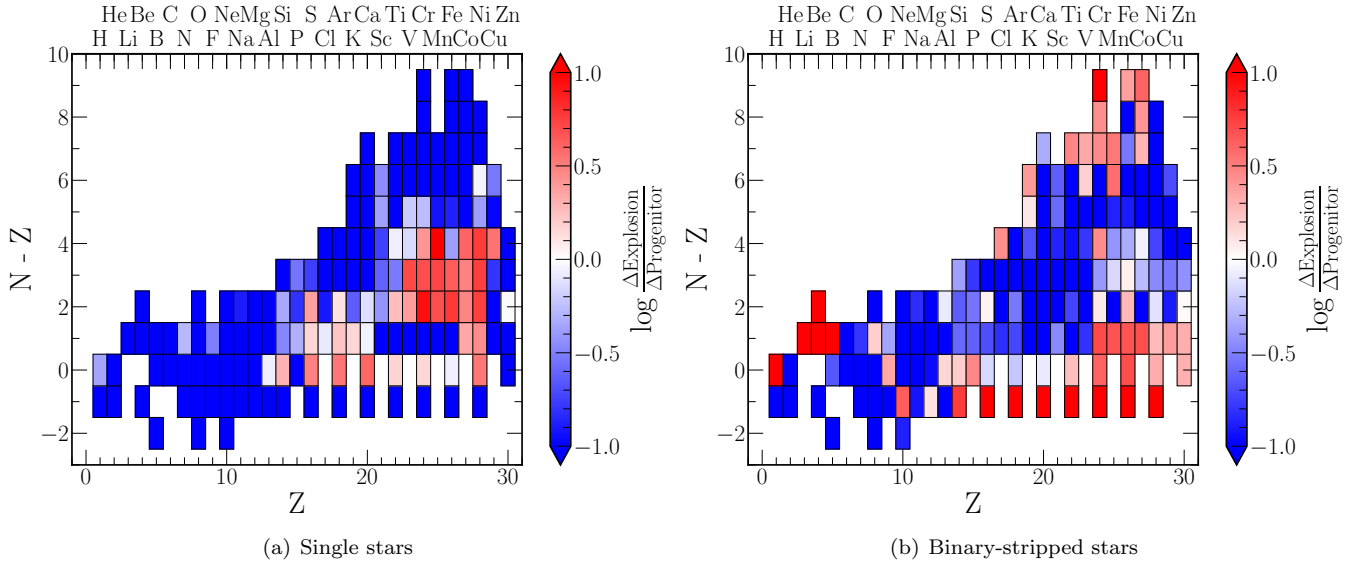


Figure 7. The logarithmic ratio of the variation in the isotopic ejecta when considering the uncertainties in explosion physics ($\Delta\text{Explosion}$) and the uncertainties in the progenitors ($\Delta\text{Progenitor}$). $\Delta\text{Explosion}$ is defined as the spread in the final ejecta composition for a $17 M_{\odot}$ model when the explosion physics is varied. $\Delta\text{Progenitor}$ is the spread in the final ejecta composition for all models that explode with fixed explosion physics, varying the initial mass of the progenitor. The colors are truncated to be between -1 and 1.

In [Andrews et al. \(2020\)](#) a number of isotopes (^{43}K , ^{47}Ca , ^{44}Sc , ^{47}Sc , ^{48}V , ^{48}Cr , ^{51}Cr , ^{52}Mn , ^{59}Fe , ^{56}Co , ^{57}Co , and ^{57}Ni) were determined to be interesting candidates for next-generation gamma-ray detectors. This was due to their accessible gamma-ray energies as well as their sensitivity to the structure of the progenitor (^{48}V and ^{57}Co) or the explosion energy (^{43}K , ^{47}Ca , ^{44}Sc , ^{47}Sc , ^{59}Fe).

If we assume the (arbitrary) point of $\log(\Delta\text{Explosion}/\Delta\text{Progenitor}) > 0.1$ as the point where isotopes are probing for the explosion mechanism (instead of them profiling the stellar structure) we can then use the isotope list of [Andrews et al. \(2020\)](#) to determine whether these isotopes are interesting for our binary-stripped stars. We find that the following are interesting isotopes, by that definition, for probing the explosion properties in single stars: ^{48}V , ^{48}Cr , ^{51}Cr , ^{52}Mn , ^{56}Co , ^{57}Co , and ^{57}Ni , while for binaries it is: ^{44}Sc , ^{48}Cr , ^{59}Fe , ^{57}Co , and ^{57}Ni . Note that the two lists do not overlap, nor does each isotope have the same level of sensitivity to the explosion between single and binary-stripped stars. We find ^{48}V and ^{52}Mn are much stronger probes of the explosion physics in single stars than in binaries, while ^{48}Cr is more sensitive to the explosion mechanism in binaries than in singles.

6. CAVEATS

6.1. ^{26}Al

^{26}Al is a short-lived isotope that decays to an excited state of ^{26}Mg . This excited ^{26}Mg then rapidly emits a

1.81 MeV γ -ray. Given the the short half life of ^{26}Al , its detection in the Galaxy requires a continuous production source ([Diehl et al. 2010](#)). ^{26}Al has multiple formation sites inside stars, mainly via proton captures onto ^{25}Mg ([Limongi & Chieffi 2006](#)). However, ^{26}Al has several isomers which complicate the decay chain. The ground state of ^{26}Al decays to ^{26}Mg with a half life of ~ 700 kyr, however the excited state of ^{26}Al decays to ^{26}Mg in ~ 6 seconds ([Misch et al. 2021](#)). At the temperatures found in stellar envelopes, excited ^{26}Al decays to ^{26}Mg before it can de-excite back to its ground state, this rapidly converts most of the ^{26}Al into ^{26}Mg . Our nuclear network does not contain the ^{26}Al isomers, with the decay rate of ^{26}Al only considering the ground state transitions. Thus we significantly over produce the amount of ^{26}Al in our wind yields and RLOF ejecta (see for instance the models of [Brinkman et al. \(2019, 2021\)](#) for ^{26}Al yields from binary stars). This over production ranges from a factor 10 to 10,000 depending on the initial mass, with low mass stars having larger over-production factors. Thus we can make no statement on the production of ^{26}Al in stellar winds, without further post-processing of the chemical yields. Tests with a nuclear network that contains the ^{26}Al isomers give wind and RLOF results that are consistent with those of [Brinkman et al. \(2021\)](#). In our models we have ^{26}Mg wind yields of $M \approx 10^{-3} M_{\odot}$, while ^{26}Al wind yields of $M \approx 10^{-4} M_{\odot}$ (at $M_{\text{init}} \approx 20 M_{\odot}$). Thus the lack of ^{26}Al excited-state decays to ^{26}Mg leads to a systematic

change of order 10% (depending on the initial stellar mass) in the ^{26}Mg wind yields.

6.2. Neutral ion electron captures

MESA’s default reaction rate for $^7\text{Be}(e^-, \nu_e)^7\text{Li}$ (for version r12115) came from REACLIB (Cyburt et al. 2010). However, REACLIB is only defined for temperatures above $T > 10^7\text{K}$, thus it assumes that all atoms are ionised. While this is a reasonable assumption for most rates, which occur deep in the stellar interior, significant lithium production occurs in stellar envelopes with temperatures below $T < 10^7\text{K}$ where the reaction rate can then depend on the level of ionisation (Schwab 2020). This has been corrected in MESA version 2c2ad6c by switching to the rate of Simonucci et al. (2013) which includes this effect, but this was not available in MESA for this work. We caution against making any inferences for either ^7Be or ^7Li from this work. Other isotopes that are sensitive to the level of ionisation may also be affected, if their rates are provided by REACLIB.

7. DISCUSSION

We have used in this work the default MESA set of reaction rates, which is a mix of rates from NACRE and JINA’s REACLIB (Angulo et al. 1999; Cyburt et al. 2010). These rates in turn are based on experimental data and thus have experimental errors associated with them (Sallaska et al. 2013). Changes in the nuclear reaction rates can have two different effects on the resulting nucleosynthesis, directly changing the amount of a species produced (Bliss et al. 2020; Subedi et al. 2020; Sieverding et al. 2022), and secondly indirectly by changing stellar properties like the core mass (Brown et al. 1999, 2001; West et al. 2013; Fields et al. 2018; Sukhbold & Adams 2020; Farmer et al. 2020). Of critical importance is the $^{12}\text{C}(\alpha, \gamma)^{16}\text{O}$ reaction (deBoer et al. 2017; Farmer et al. 2020) during core helium burning. Variations within its known uncertainties can lead to core masses changing by $\pm 2 M_\odot$ (Sukhbold & Adams 2020) and central carbon fractions by $\pm 80\%$ (Fields et al. 2016, 2018). This can alter models such that they change from exploding to non-exploding, significantly changing the final yields. Observations of WO stars suggest that the $^{12}\text{C}(\alpha, \gamma)^{16}\text{O}$ reaction needs a reduction by up to 50% to match the observed C/O ratio (Aadland et al. 2022). Further work is needed to integrate reaction rate uncertainties, for all reaction rates, into stellar models.

Significant uncertainties remain in the treatment of mass transfer between binaries (e.g. Klencki et al. 2020, 2022; Sen et al. 2022), whether the stars lose their entire hydrogen envelopes (Götberg et al. 2017; Yoon et al.

2017; Laplace et al. 2020), and how much of the material lost by the donor is accreted by the companion (de Mink et al. 2009; Janssens et al. 2021). In this work we have assumed fully conservative mass transfer (all material lost is accreted by the companion), if mass transfer was not fully conservative (some mass is lost during RLOF) then the Universe can be enriched with those products lost from the hydrogen envelope (see Section 4.2).

Related to whether a star fully strips during RLOF is the wind mass loss, and its scaling with the metallicity. Lower wind mass loss rates, either intrinsically or due to lower metallicities (Sander et al. 2020; Sander & Vink 2020), may allow stars to keep part of their hydrogen envelopes (Götberg et al. 2017; Yoon et al. 2017; Laplace et al. 2020). If a star keeps its hydrogen envelope then the yields for the higher-mass elements seen in Figure 1(a) will decrease as the star will not expose its helium core. At low metallicities, binary stars may not become fully stripped (Götberg et al. 2017; Yoon et al. 2017; Laplace et al. 2020; Klencki et al. 2022), this would lead to the binary stars having yields closer to those of single stars.

We modelled our binaries as Case B systems, where stable RLOF occurs during the Hertzsprung gap. Depending on the initial period, binaries can also interact earlier during the main sequence (Case A) or later during core helium burning (Case C). Interaction during Case A RLOF is likely to lead to a smaller core mass (Schneider et al. 2021), which would then be more likely to explode successfully in a SN. While interaction during Case C may occur too late in the star’s life to significantly affect the core evolution. Though, if the star was likely to form a BH, then Case C mass loss will liberate some of the envelope that would have otherwise collapsed into the BH.

The consequences of stellar mergers for the final structure also depend on the timing of the merger. Mergers which occur when both stars are on the main sequence (MS) are expected to increase the core mass of the resulting star, as compared to that of the primary star in the pre-merger binary, and the later evolution would likely be approximately described by that of an initially more massive single star (although see, e.g., Renzo et al. 2022 for details of the structure which may also differ for post-merger stars). For post-MS mergers, any erosion of the hydrogen-depleted core — either during the merger (e.g. Ivanova & Podsiadlowski 2003) or by dredge-out during post-merger relaxation (Justham et al. 2014) — would not be reversed by growth of a convective MS core. The consequences of this decrease in core mass may make many such merger products more explodable

than the primary star would have become if single, despite the increase in stellar mass (Justham et al. 2014).

We have ignored the evolution of the accretor in this work. Their most significant contribution would likely be due to the mass gain, moving stars that are initially too light to explode ($M_{\text{init}} \approx 6 - 8 M_{\odot}$) to gain enough mass that they now explode (Podsiadlowski et al. 2004; Zapartas et al. 2017, 2019). Secondly, their contribution will depend on how much of the mass that they accreted, remains bound to the accretor and is further processed inside the accretor. For instance, SN 2016bkv shows nucleosynthetic signals that it may have accreted material, but with no significant reprocessing of the accreted material (Deckers et al. 2021). Detailed modelling of the nucleosynthetic signature of accretors is deferred to later work.

We modelled our stars as non-rotating objects, however rotation can play a key role in the evolution of massive stars (Meynet & Maeder 2000). This is due to both changes in the core structure (Ekström et al. 2012; Murphy et al. 2021), chemical mixing of elements to the surface (Meynet et al. 2006; Groh et al. 2019), and changes to the observed chemical composition (Hunter et al. 2007, 2008, 2009). Indeed, rotation may be needed to explain s-process enrichment in the Solar system (Rizuti et al. 2019, 2021; Prantzos et al. 2020). Rotation will also play a role during the explosion, and whether the compact object forms a jet which may alter the final nucleosynthetic signal (Winteler et al. 2012; Reichert et al. 2023).

8. CONCLUSION

Motivated by the differences we found in the ^{12}C yields in Farmer et al. (2021) we have extended our study of the nucleosynthesis of massive binary-stripped and single stars with a larger nuclear network. With the high fraction of massive stars being inferred to be in binaries, accurate modelling of binary evolution is needed to be able to predict the nucleosynthetic yields of massive stars.

To achieve this we have modelled the evolution of binary-stripped and single stars from the onset of hydrogen burning to core collapse, at solar metallicity. We have then modelled the nucleosynthetic yields due to the supernovae shock. This was done using a large 162-isotope nuclear network for all phases of the star’s evolution.

A. OTHER PHYSICS CHOICES

MESA depends on a number of sources for its microphysics; with its EOS being a blend of several sources;

Our results can be summarised as follows:

- We find that, in general, stars stripped in binaries synthesize and then eject more mass of all elements than single stars. The increase in the yields depends strongly on the isotope. This is due to the increased mass loss in binary-stripped stars ejecting more material during the star’s evolution and binary-stripped stars being more explodable and thus ejecting more material during the supernovae.
- $^{13}\text{C}/^{12}\text{C}$ from massive stars may provide information on the efficiency of mass transfer. This is because ^{13}C is primarily only ejected during RLOF, while ^{12}C is ejected primarily during WR wind mass loss.
- In qualitative agreement with previous work, we find that stars stripped in binaries are somewhat more likely to successfully explode in a core-collapse supernova, especially at higher masses. This is due to the changes in the core mass due to the mass loss in RLOF.
- Depending on the element, the difference between single and binary-stripped stars can be as large as the difference between different software instruments. However, we stress we have not attempted to calibrate our results to observations.
- We have identified a number of radioactive isotopes that may prove useful in constraining the explosion mechanism or progenitor structure with next generation gamma-ray detectors.
- In the online Zenodo material we provide tables of chemical yields for all isotopes for all types of mass loss.

We conclude that the yields from massive binary-stripped stars are different from those of massive single stars, and that this difference depends on the isotope. Thus there is no single scale factor for taking into account of binary interactions on the chemical yields. Therefore the effects of binarity require explicit modelling of all isotopes that are of interest.

APPENDIX

OPAL (Rogers & Nayfonov 2002), SCVH (Saumon et al. 1995), PTEH (Pols et al. 1995b), HELM (Timmes &

Swesty 2000), and PC (Potekhin & Chabrier 2010). While opacities are primarily from OPAL (Iglesias & Rogers 1993, 1996) with additional data from Buchler & Yueh (1976); Ferguson et al. (2005); Cassisi et al. (2007)

The nuclear reaction rates are a combination of NACRE and JINA’s REACLIB (Angulo et al. 1999; Cyburt et al. 2010) compilations. Additional weak reaction rates are from Fuller et al. (1985); Oda et al. (1994); Langanke & Martínez-Pinedo (2000). Screening of the nuclear reaction rates is computed with the prescription of Chugunov et al. (2007). Thermal neutrino loss rates are provided from the fits of Itoh et al. (1996). The Roche lobe radii in binary systems is computed from the fit of Eggleton (1983). In our Roche lobe overflowing binary systems we compute the mass loss rate using the the prescription of Kolb & Ritter (1990).

B. DATA TABLES

Table 2 shows the ^{19}F yields from our models. This includes both the wind mass loss, RLOF, and supernovae yields. We provide supernova yields for all models, as there are multiple different criteria that can be used to determine whether a star successfully ejects its envelope in a supernovae. The online Zenodo material contains yield tables for all 162-isotopes from our nuclear network.

C. WIND SENSITIVITY

Figure 8 shows the ratio of the ^{12}C yields between a $45 M_{\odot}$ binary-stripped and single star as a function of the wind scale factor η_{Dutch} . As η_{Dutch} increases the total wind mass loss increases. This increases the amount of the C/O rich helium core removed once the star is stripped of its hydrogen and helium layers. For all $\eta_{\text{Dutch}} > 0.5$ binary-stripped stars produce more ^{12}C than single stars, with a peak in the fraction coming from binaries at $\eta_{\text{Dutch}} \approx 0.8$. This is due to the single star not removing its helium layers and thus not exposing its C/O rich helium core, while the binary star does (Farmer et al. 2021). The online Zenodo material contains the wind yields for all isotopes, for a $M_{\text{init}} = 45 M_{\odot}$ single and binary-stripped stars.

D. EVOLUTION PROPERTIES

Tables 3 and 4 detail the main properties of our stellar models during their evolution.

E. EXPLOSION PROPERTIES

Tables 5 and 6 detail the main properties of our stellar models during the core collapse phase of their evolution.

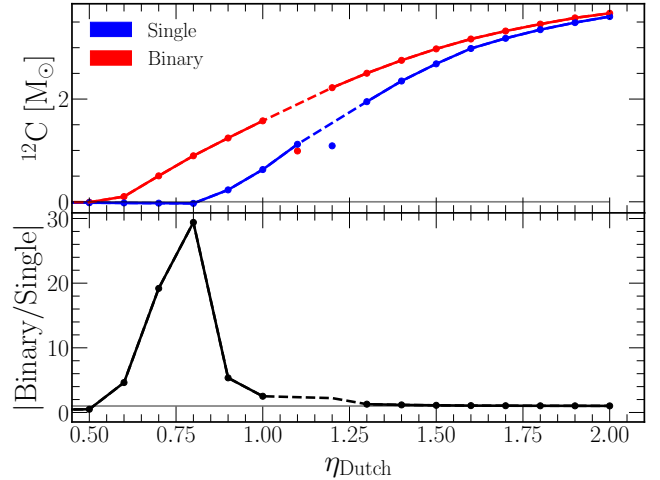


Figure 8. The top panel shows the ^{12}C yield in solar masses for $M_{\text{init}}=45 M_{\odot}$, single (blue) and binary (red), stars as a function of the wind scaling factor η_{Dutch} . The grey line in this panel shows a value of zero. The bottom panels shows the absolute values of the ratio of the two yields. Two models are shown that have anomalous behaviour and are excluded from the curves. The grey line in this panel shows where the ratio equals one.

Table 2. A representative sample of the data available. Data is available online for all 162 isotopes. The amount of ^{19}F ejected in solar masses broken down by mass-loss type for both single stars and the primary star in the binary. “Init” marks the amount that is from the initial composition of the star. All ejecta masses are in units of 10^{-5} solar masses. Blank values indicate models that did not evolve successfully to core collapse. We have included the supernova yields from all models, assuming all models successfully explode.

Initial mass [M_{\odot}]	Single [$10^{-5} M_{\odot}$]				Binary [$10^{-5} M_{\odot}$]					
	M_{Winds}	$M_{\text{Winds,init}}$	M_{CC}	$M_{\text{CC,init}}$	M_{Winds}	$M_{\text{Winds,init}}$	M_{RLOF}	$M_{\text{RLOF,init}}$	M_{CC}	$M_{\text{CC,init}}$
11	0.051	0.058	1.262	0.276	0.009	0.025	0.209	0.251	0.265	0.064
12	0.070	0.079	0.206	0.287	0.011	0.031	0.222	0.266	1.459	0.076
13	0.092	0.104	1.045	0.299	0.013	0.037	0.234	0.280	1.248	0.089
14	0.118	0.135	0.888	0.298	0.015	0.045	0.245	0.293	0.120	0.097
15	0.149	0.170	0.256	0.293	0.017	0.054	0.255	0.306	0.622	0.111
16	0.183	0.211	0.232	0.291	0.021	0.063	0.263	0.320	0.849	0.122
17	0.210	0.245	0.266	0.300	0.024	0.075	0.271	0.330	0.238	0.135
18	0.235	0.279	0.345	0.298	0.028	0.086	0.277	0.345	0.384	0.143
19	0.244	0.298	0.475	0.318	0.033	0.096	0.282	0.363	0.794	0.152
20	0.235	0.297	0.621	0.347	0.040	0.074	0.286	0.382	0.375	0.192
21	0.243	0.315	0.642	0.363	0.047	0.090	0.284	0.391	0.432	0.199
22	0.273	0.356	0.585	0.360	0.061	0.086	0.267	0.363	0.271	0.262
23	0.323	0.421	1.268	0.310	0.068	0.095	0.275	0.381	0.240	0.264
24	0.337	0.447	10.390	0.328						
25	0.331	0.434	1.472	0.378						
26	0.367	0.496	1.539	0.348	0.086	0.189	0.283	0.399	2.250	0.259
27	0.374	0.514	1.001	0.365	0.110	0.170	0.248	0.355	1.323	0.357
28	0.371	0.532	0.706	0.382						
29	0.382	0.550	0.732	0.402						
30	0.379	0.555	0.780	0.433	0.134	0.264	0.240	0.366	6.873	0.367
31	0.395	0.575	0.853	0.445	0.147	0.238	0.248	0.373	0.972	0.413
32	0.397	0.593	1.352	0.460	0.149	0.329	0.252	0.385	28.069	0.339
33	0.408	0.650	1.943	0.435	0.264	0.355	0.257	0.386	1.573	0.346
34	0.412	0.661	2.232	0.464	0.207	0.380	0.245	0.370	1.518	0.375
35	0.419	0.695	32.298	0.468	0.678	0.409	0.240	0.385	1.527	0.366
36	0.422	0.737	0.913	0.453	0.635	0.431	0.224	0.389	1.293	0.376
37	0.461	0.749	1.396	0.476	1.343	0.477	0.228	0.366	1.398	0.391
38	0.529	0.770	1.416	0.489	1.420	0.501	0.219	0.362	1.516	0.409
39	0.624	0.793	1.415	0.500	1.519	0.529	0.208	0.357	1.499	0.423
40	0.696	0.815	1.319	0.516	1.566	0.554	0.198	0.352	1.541	0.435
41	0.792	0.838	1.250	0.544	1.628	0.581	0.188	0.347	1.432	0.446
42	0.905	0.863	1.328	0.549	1.703	0.610	0.176	0.340	1.496	0.471
43	0.994	0.886	1.243	0.561	1.743	0.638	0.163	0.333	1.217	0.467
44	1.096	0.911	2.062	0.582	1.967	0.687	0.150	0.318	1.375	0.485
45	1.175	0.934	1.293	0.591	1.998	0.715	0.137	0.310	1.211	0.504

Table 3. Properties of our single star models during their evolution. M_{init} is the initial mass, M_{Final} is the final mass of the star, Age is the total lifetime of the star, He_{core} is the helium core mass at collapse, C_{core} is the carbon core mass at collapse, ΔM_{wind} is the mass lost due to winds, ΔM_{RLOF} is the mass loss due to RLOF, $^{12}\text{C}_{\text{cntr}}$ is the central ^{12}C fraction at core helium depletion, H_{fin} , He_{fin} , C_{fin} are the final mass of ^1H , ^4He , and ^{12}C at collapse.

M_{init} M_{\odot}	M_{Final} M_{\odot}	Age Myr	He_{core} M_{\odot}	C_{core} M_{\odot}	ΔM_{wind} M_{\odot}	ΔM_{RLOF} M_{\odot}	$^{12}\text{C}_{\text{cntr}}$	H_{fin} M_{\odot}	He_{fin} M_{\odot}	C_{fin} M_{\odot}
11	9.36	23.59	3.78	2.34	1.64	0.00	0.33	3.82	2.98	0.13
12	9.77	20.38	4.27	2.75	2.23	0.00	0.32	3.75	3.04	0.12
13	10.04	17.95	4.78	3.16	2.96	0.00	0.31	3.58	3.07	0.18
14	10.18	16.06	5.29	3.61	3.82	0.00	0.30	3.30	3.05	0.18
15	10.18	14.55	5.82	4.07	4.82	0.00	0.30	2.91	2.98	0.17
16	10.03	13.32	6.36	4.54	5.97	0.00	0.29	2.41	2.86	0.18
17	10.05	12.30	6.85	4.99	6.95	0.00	0.28	2.07	2.78	0.19
18	10.08	11.45	7.34	5.44	7.92	0.00	0.28	1.74	2.70	0.31
19	10.55	10.73	7.76	5.82	8.45	0.00	0.27	1.75	2.76	0.27
20	11.57	10.11	8.04	6.08	8.43	0.00	0.27	2.22	3.05	0.32
21	12.05	9.58	8.42	6.39	8.95	0.00	0.27	2.26	3.17	0.32
22	11.90	9.12	8.78	6.74	10.10	0.00	0.26	1.81	3.13	0.34
23	11.05	8.72	9.41	7.32	11.95	0.00	0.24	0.73	2.80	0.20
24	11.31	8.35	9.15	7.81	12.69	0.00	0.23	0.57	2.75	0.30
25	12.68	8.02	10.35	8.20	12.32	0.00	0.23	1.05	3.23	0.30
26	11.94	7.72	11.70	9.47	14.06	0.00	0.21	0.05	2.20	0.37
27	12.42	7.46	11.98	9.73	14.58	0.00	0.21	0.11	2.39	0.41
28	12.89	7.23	12.15	9.87	15.11	0.00	0.21	0.23	2.60	0.39
29	13.38	7.01	12.62	10.31	15.62	0.00	0.20	0.24	2.64	0.43
30	14.26	6.80	13.09	10.73	15.74	0.00	0.20	0.40	2.92	0.31
31	14.68	6.61	12.80	11.70	16.32	0.00	0.20	0.16	2.60	0.30
32	15.16	6.44	14.41	11.98	16.84	0.00	0.20	0.23	2.72	0.24
33	14.57	6.29	14.57	12.66	18.43	0.00	0.20	0.00	1.56	0.57
34	15.24	6.14	15.24	13.60	18.76	0.00	0.20	0.00	1.59	0.64
35	15.27	6.01	15.27	^a	19.73	0.00	0.20	0.00	1.18	0.91
36	15.11	5.88	15.11	^a	20.89	0.00	0.20	0.00	0.82	0.66
37	15.75	5.74	15.75	13.74	21.25	0.00	0.20	0.00	0.14	1.11
38	16.16	5.63	16.16	12.44	21.84	0.00	0.20	0.00	0.13	1.20
39	16.51	5.53	16.51	10.74	22.49	0.00	0.20	0.00	0.15	1.20
40	16.89	5.44	16.89	14.23	23.11	0.00	0.20	0.00	0.28	1.19
41	17.23	5.35	17.23	14.82	23.77	0.00	0.20	0.00	0.19	1.21
42	17.53	5.26	17.53	14.31	24.47	0.00	0.19	0.00	0.21	1.28
43	17.86	5.18	17.86	9.57	25.14	0.00	0.19	0.00	0.19	1.24
44	18.16	5.10	18.16	7.30	25.84	0.00	0.19	0.00	0.22	2.00
45	18.50	5.03	18.50	15.84	26.50	0.00	0.19	0.00	0.14	1.35

^aThe C core mass is ill-defined due to convective mixing blurring the chemical gradient at the edge of the C core in these models.

Table 4. Properties of our binary-stripped stars during their evolution. Columns have the same meaning as in Table 3.

M_{init} M_{\odot}	M_{Final} M_{\odot}	Age Myr	He_{core} M_{\odot}	C_{core} M_{\odot}	ΔM_{wind} M_{\odot}	ΔM_{RLOF} M_{\odot}	$^{12}\text{C}_{\text{ctr}}$	H_{fin} M_{\odot}	He_{fin} M_{\odot}	C_{fin} M_{\odot}
11	3.17	23.69	3.17	1.93	0.70	7.12	0.38	0.00	1.16	0.06
12	3.58	20.44	3.58	2.22	0.87	7.55	0.37	0.00	1.24	0.08
13	3.98	17.99	3.98	2.55	1.06	7.95	0.36	0.00	1.28	0.16
14	4.39	16.08	4.39	2.88	1.29	8.32	0.35	0.00	1.35	0.11
15	4.79	14.56	4.79	3.23	1.54	8.67	0.34	0.00	1.33	0.19
16	5.15	13.33	5.15	3.56	1.78	9.07	0.33	0.00	1.34	0.22
17	5.52	12.31	5.52	3.91	2.13	9.35	0.32	0.00	1.31	0.22
18	5.77	11.46	5.77	4.14	2.43	9.80	0.32	0.00	1.31	0.25
19	6.00	10.75	6.00	4.36	2.71	10.29	0.31	0.00	1.19	0.35
20	7.07	10.12	7.07	5.27	2.09	10.83	0.29	0.00	1.39	0.36
21	7.36	9.58	7.36	5.55	2.56	11.08	0.29	0.00	1.36	0.35
22	9.27	9.15	8.48	6.49	2.43	10.30	0.25	0.32	2.31	0.35
23	9.50	8.71	7.44	7.09	2.70	10.80	0.26	0.14	2.12	0.40
24										
25										
26	9.31	7.70	9.31	7.46	5.37	11.32	0.27	0.00	0.86	0.84
27	12.12	7.47	11.15	8.97	4.81	10.07	0.23	0.36	2.58	0.33
28										
29										
30	12.12	6.79	12.12	0.00	7.50	10.38	0.23	0.00	1.33	0.72
31	13.66	6.61	12.43	11.15	6.75	10.58	0.21	0.03	2.26	0.21
32	11.75	6.43	11.75	9.72	9.32	10.93	0.24	0.00	0.38	1.04
33	11.98	6.28	11.98	9.91	10.08	10.94	0.23	0.00	0.29	1.14
34	12.71	6.14	12.71	10.53	10.78	10.51	0.23	0.00	0.27	1.22
35	12.47	6.00	12.47	10.32	11.60	10.93	0.23	0.00	0.30	1.22
36	12.73	5.88	12.73	10.55	12.24	11.04	0.23	0.00	0.29	1.25
37	13.11	5.75	13.11	10.89	13.52	10.37	0.22	0.00	0.28	1.29
38	13.50	5.64	13.50	6.22	14.22	10.28	0.22	0.00	0.17	1.12
39	13.86	5.54	13.86	6.31	15.00	10.14	0.22	0.00	0.20	1.19
40	14.29	5.44	14.29	6.55	15.72	9.99	0.21	0.00	0.20	1.23
41	14.69	5.35	14.69	7.22	16.48	9.83	0.21	0.00	0.19	1.21
42	15.06	5.27	15.06	6.49	17.29	9.65	0.21	0.00	0.19	1.28
43	15.48	5.19	15.48	12.92	18.09	9.43	0.21	0.00	0.30	1.21
44	15.49	5.11	15.49	7.01	19.49	9.01	0.21	0.00	0.18	1.22
45	15.91	5.04	15.91	9.77	20.29	8.80	0.20	0.00	0.21	1.28

Table 5. Properties of our single star models during the supernovae explosion. M_{init} is the initial mass, M_{Final} is the final mass of the star, M_{Fe} is the mass of the iron core, M_{Ni56} is the mass of ^{56}Ni at the time of shock breakout, E is the total energy of the model at shock breakout, M_{rem} is the mass of the compact object at shock breakout (assuming the envelope did not fallback onto the compact object), Fate is the final fate as given by [Ertl et al. \(2016\)](#).

M_{init}	M_{Final}	M_{Fe}	$\xi_{M=2.5}$	M_4	μ_4	M_{Ni56}	E	M_{rem}	Fate
M_{\odot}	M_{\odot}	M_{\odot}		M_{\odot}	$M_{\odot}/1000\text{km}$	M_{\odot}	10^{51}erg/s	M_{\odot}	
11	9.36	1.36	0.05	1.52	0.06	0.04	1.00	1.53	NS
12	9.77	1.35	0.09	1.62	0.05	0.02	1.00	1.62	NS
13	10.04	1.40	0.18	1.57	0.10	0.08	1.00	1.57	BH
14	10.18	1.43	0.22	1.73	0.10	0.04	1.00	1.73	BH
15	10.18	1.47	0.19	1.88	0.07	0.04	1.00	1.88	NS
16	10.03	1.47	0.22	1.77	0.10	0.06	1.00	1.78	BH
17	10.05	1.41	0.17	1.56	0.12	0.14	1.00	1.56	BH
18	10.08	1.39	0.19	1.62	0.08	0.04	1.00	1.62	BH
19	10.55	1.40	0.18	1.53	0.10	0.11	1.00	1.53	BH
20	11.57	1.44	0.21	1.71	0.09	0.06	1.00	1.71	BH
21	12.05	1.41	0.16	1.75	0.06	0.02	1.00	1.75	NS
22	11.90	1.43	0.15	1.68	0.08	0.08	1.00	1.68	BH
23	11.05	1.64	0.41	2.27	0.12	0.07	1.00	2.27	BH
24	11.31	1.70	0.51	2.02	0.27	0.31	1.00	2.02	BH
25	12.68	1.71	0.53	1.96	0.30	0.39	1.00	1.96	BH
26	11.94	1.61	0.39	2.08	0.14	0.14	1.00	2.08	BH
27	12.42	1.62	0.38	2.06	0.14	0.13	1.00	2.06	BH
28	12.89	1.62	0.38	2.06	0.14	0.13	1.00	2.06	BH
29	13.38	1.57	0.34	1.98	0.12	0.13	1.00	1.98	BH
30	14.26	1.49	0.26	1.99	0.09	0.06	1.00	1.99	NS
31	14.68	1.51	0.25	2.07	0.07	0.06	1.00	2.07	NS
32	15.16	1.53	0.26	2.12	0.07	0.05	1.00	2.12	NS
33	14.57	1.65	0.44	2.22	0.15	0.17	1.00	2.22	BH
34	15.24	1.67	0.49	2.09	0.25	0.30	1.00	2.09	BH
35	15.27	1.51	0.29	2.00	0.13	0.12	1.00	2.00	BH
36	15.11	1.60	0.37	2.25	0.10	0.08	1.00	2.25	NS
37	15.75	1.57	0.33	2.24	0.08	0.07	1.00	2.24	NS
38	16.16	1.58	0.34	2.28	0.08	0.05	1.00	2.28	NS
39	16.51	1.58	0.37	2.32	0.08	0.06	1.00	2.32	NS
40	16.89	1.61	0.44	2.26	0.15	0.14	1.01	2.26	BH
41	17.23	1.57	0.40	1.79	0.21	0.33	1.00	1.79	BH
42	17.53	1.59	0.42	1.96	0.20	0.26	1.00	1.96	BH
43	17.86	1.58	0.43	1.94	0.22	0.28	1.00	1.94	BH
44	18.16	1.49	0.33	1.66	0.19	0.30	1.00	1.66	BH
45	18.50	1.55	0.38	1.74	0.19	0.33	1.00	1.74	BH

Table 6. Properties of our binary-stripped models during the supernovae explosion. Columns have the same meaning as in Table 5.

M_{init} M_{\odot}	M_{Final} M_{\odot}	M_{Fe} M_{\odot}	$\xi_{M=2.5}$	M_4 M_{\odot}	μ_4	M_{Ni56} M_{\odot}	E 10^{51}erg/s	M_{rem} M_{\odot}	Fate
11	3.17	1.26	0.01	1.36	0.03	0.03	1.00	1.36	NS
12	3.58	1.32	0.03	1.43	0.06	0.08	1.00	1.43	NS
13	3.98	1.32	0.10	1.46	0.06	0.07	1.00	1.46	NS
14	4.39	1.35	0.10	1.64	0.04	0.02	1.00	1.64	NS
15	4.79	1.40	0.18	1.64	0.08	0.08	1.00	1.64	BH
16	5.15	1.46	0.21	1.69	0.10	0.12	1.00	1.69	BH
17	5.52	1.44	0.17	1.69	0.08	0.11	1.00	1.69	BH
18	5.77	1.44	0.19	1.71	0.09	0.11	1.00	1.71	BH
19	6.00	1.43	0.19	1.69	0.09	0.10	1.00	1.69	BH
20	7.07	1.38	0.21	1.62	0.10	0.11	1.00	1.62	BH
21	7.36	1.44	0.20	1.70	0.09	0.10	1.00	1.70	BH
22	9.27	1.46	0.17	1.85	0.06	0.06	1.00	1.85	NS
23	9.50	1.51	0.23	2.03	0.08	0.06	1.00	2.03	NS
24									
25									
26	9.31	1.58	0.34	1.96	0.15	0.16	1.00	1.96	BH
27	12.12	1.69	0.50	1.99	0.26	0.34	1.00	1.99	BH
28									
29									
30	12.12	1.38	0.13	1.71	0.05	0.03	1.00	1.71	NS
31	13.66	1.43	0.18	1.95	0.06	0.02	1.00	1.95	NS
32	11.75	1.69	0.49	2.13	0.22	0.26	1.01	2.13	BH
33	11.98	1.65	0.46	2.15	0.19	0.21	1.00	2.15	BH
34	12.71	1.62	0.39	2.08	0.14	0.15	1.00	2.08	BH
35	12.47	1.62	0.39	2.09	0.14	0.15	1.00	2.09	BH
36	12.73	1.61	0.38	2.06	0.14	0.15	1.00	2.06	BH
37	13.11	1.60	0.36	2.03	0.13	0.14	1.00	2.03	BH
38	13.50	1.45	0.18	1.90	0.06	0.06	1.00	1.90	NS
39	13.86	1.46	0.19	1.87	0.08	0.10	1.00	1.87	NS
40	14.29	1.48	0.20	1.94	0.07	0.08	1.00	1.94	NS
41	14.69	1.49	0.22	2.03	0.07	0.07	1.00	2.03	NS
42	15.06	1.48	0.21	1.69	0.14	0.20	1.00	1.69	BH
43	15.48	1.58	0.32	2.24	0.08	0.05	1.00	2.24	NS
44	15.49	1.51	0.23	1.73	0.14	0.20	1.00	1.73	BH
45	15.91	1.47	0.28	1.60	0.19	0.32	1.00	1.60	BH

ACKNOWLEDGMENTS

We acknowledge helpful discussions with M. Renzo. SdM and SJ acknowledge funding by the Netherlands Organization for Scientific Research (NWO) as part of the Vidi research program BinWaves (project number 639.042.728). This work was also supported by the Cost Action Program ChETEC CA16117. EL acknowledges funding from the European Research Council (ERC) under the European Union’s Horizon 2020 research and innovation programme (Grant agreement No. 945806). This research has made use of NASA’s Astrophysics Data System.

Software: `mesaPlot` (Farmer 2018), `mesaSDK` (Townsend 2019), `ipython/jupyter` (Pérez & Granger 2007; Kluver et al. 2016), `matplotlib` (Hunter 2007), `NumPy` (van der Walt et al. 2011), `Parallel` (Tange 2021), `VICE` (Johnson & Weinberg 2020; Johnson et al. 2021; Griffith et al. 2021), `MESA` (Paxton et al. 2011, 2013, 2015, 2018, 2019; Jermyn et al. 2022), `pyMesa` (Farmer & Bauer 2018), and `Webplotdigitizer` (Rohatgi 2022).

REFERENCES

- Aadland, E., Massey, P., John Hillier, D., et al. 2022, *ApJ*, 931, 157, doi: [10.3847/1538-4357/ac66e7](https://doi.org/10.3847/1538-4357/ac66e7)
- Abate, C., Pols, O. R., Karakas, A. I., & Izzard, R. G. 2015, *A&A*, 576, A118, doi: [10.1051/0004-6361/201424739](https://doi.org/10.1051/0004-6361/201424739)
- Abt, H. A. 1983, *ARA&A*, 21, 343
- Andrews, S., Fryer, C., Even, W., Jones, S., & Pignatari, M. 2020, *ApJ*, 890, 35, doi: [10.3847/1538-4357/ab64f8](https://doi.org/10.3847/1538-4357/ab64f8)
- Angulo, C., Arnould, M., Rayet, M., et al. 1999, *NuPhA*, 656, 3, doi: [10.1016/S0375-9474\(99\)00030-5](https://doi.org/10.1016/S0375-9474(99)00030-5)
- Arnould, M., Goriely, S., & Jorissen, A. 1999, *A&A*, 347, 572. <https://arxiv.org/abs/astro-ph/9904407>
- Arnould, M., Goriely, S., & Takahashi, K. 2007, *PhR*, 450, 97, doi: [10.1016/j.physrep.2007.06.002](https://doi.org/10.1016/j.physrep.2007.06.002)
- Arnould, M., & Takahashi, K. 1999, *Reports on Progress in Physics*, 62, 395, doi: [10.1088/0034-4885/62/3/003](https://doi.org/10.1088/0034-4885/62/3/003)
- Aufderheide, M. B., Baron, E., & Thielemann, F. K. 1991, *ApJ*, 370, 630, doi: [10.1086/169849](https://doi.org/10.1086/169849)
- Aufderheide, M. B., Fushiki, I., Woosley, S. E., & Hartmann, D. H. 1994, *ApJS*, 91, 389, doi: [10.1086/191942](https://doi.org/10.1086/191942)
- Bliss, J., Arcones, A., Montes, F., & Pereira, J. 2020, *PhRvC*, 101, 055807, doi: [10.1103/PhysRevC.101.055807](https://doi.org/10.1103/PhysRevC.101.055807)
- Boccioli, L., Roberti, L., Limongi, M., Mathews, G. J., & Chieffi, A. 2022, arXiv e-prints, arXiv:2207.08361. <https://arxiv.org/abs/2207.08361>
- Botelho, R. B., Milone, A. d. C., Meléndez, J., et al. 2020, *MNRAS*, 499, 2196, doi: [10.1093/mnras/staa2917](https://doi.org/10.1093/mnras/staa2917)
- Braun, H., & Langer, N. 1995a, *A&A*, 297, 483
- Braun, H., & Langer, N. 1995b, in *Wolf-Rayet Stars: Binaries; Colliding Winds; Evolution*, ed. K. A. van der Hucht & P. M. Williams, Vol. 163, 305
- Brinkman, H. E., den Hartogh, J. W., Doherty, C. L., Pignatari, M., & Lugaro, M. 2021, *ApJ*, 923, 47, doi: [10.3847/1538-4357/ac25ea](https://doi.org/10.3847/1538-4357/ac25ea)
- Brinkman, H. E., Doherty, C. L., Pols, O. R., et al. 2019, *ApJ*, 884, 38, doi: [10.3847/1538-4357/ab40ae](https://doi.org/10.3847/1538-4357/ab40ae)
- Brott, I., de Mink, S. E., Cantiello, M., et al. 2011, *A&A*, 530, A115, doi: [10.1051/0004-6361/201016113](https://doi.org/10.1051/0004-6361/201016113)
- Brown, G. E., Heger, A., Langer, N., et al. 2001, *NewA*, 6, 457, doi: [10.1016/S1384-1076\(01\)00077-X](https://doi.org/10.1016/S1384-1076(01)00077-X)
- Brown, G. E., Lee, C. H., & Bethe, H. A. 1999, *NewA*, 4, 313, doi: [10.1016/S1384-1076\(99\)00023-8](https://doi.org/10.1016/S1384-1076(99)00023-8)
- Brown, G. E., Weingartner, J. C., & Wijers, R. A. M. J. 1996, *ApJ*, 463, 297, doi: [10.1086/177241](https://doi.org/10.1086/177241)
- Brown, J. M., & Woosley, S. E. 2013, *ApJ*, 769, 99, doi: [10.1088/0004-637X/769/2/99](https://doi.org/10.1088/0004-637X/769/2/99)
- Buchler, J. R., & Yueh, W. R. 1976, *ApJ*, 210, 440, doi: [10.1086/154847](https://doi.org/10.1086/154847)
- Burbidge, E. M., Burbidge, G. R., Fowler, W. A., & Hoyle, F. 1957, *Reviews of Modern Physics*, 29, 547, doi: [10.1103/RevModPhys.29.547](https://doi.org/10.1103/RevModPhys.29.547)
- Busso, M., Gallino, R., & Wasserburg, G. J. 1999, *ARA&A*, 37, 239, doi: [10.1146/annurev.astro.37.1.239](https://doi.org/10.1146/annurev.astro.37.1.239)
- Carigi, L., Peimbert, M., Esteban, C., & García-Rojas, J. 2005, *ApJ*, 623, 213, doi: [10.1086/428491](https://doi.org/10.1086/428491)
- Cassisi, S., Potekhin, A. Y., Pietrinferni, A., Catelan, M., & Salaris, M. 2007, *ApJ*, 661, 1094, doi: [10.1086/516819](https://doi.org/10.1086/516819)
- Cescutti, G., Matteucci, F., McWilliam, A., & Chiappini, C. 2009, *A&A*, 505, 605, doi: [10.1051/0004-6361/200912759](https://doi.org/10.1051/0004-6361/200912759)
- Chieffi, A., & Limongi, M. 2004, *ApJ*, 608, 405, doi: [10.1086/392523](https://doi.org/10.1086/392523)
- . 2020, *ApJ*, 890, 43, doi: [10.3847/1538-4357/ab6739](https://doi.org/10.3847/1538-4357/ab6739)
- Chugunov, A. I., Dewitt, H. E., & Yakovlev, D. G. 2007, *PhRvD*, 76, 025028, doi: [10.1103/PhysRevD.76.025028](https://doi.org/10.1103/PhysRevD.76.025028)
- Crowther, P. A. 2007, *ARA&A*, 45, 177, doi: [10.1146/annurev.astro.45.051806.110615](https://doi.org/10.1146/annurev.astro.45.051806.110615)
- Cyburt, R. H., Amthor, A. M., Ferguson, R., et al. 2010, *The Astrophysical Journal Supplement Series*, 189, 240, doi: [10.1088/0067-0049/189/1/240](https://doi.org/10.1088/0067-0049/189/1/240)
- De Donder, E., & Vanbeveren, D. 2004, *NewAR*, 48, 861, doi: [10.1016/j.newar.2004.07.001](https://doi.org/10.1016/j.newar.2004.07.001)
- de Jager, C., Nieuwenhuijzen, H., & van der Hucht, K. A. 1988, *A&AS*, 72, 259
- de Mink, S. E., Cantiello, M., Langer, N., et al. 2009, *A&A*, 497, 243, doi: [10.1051/0004-6361/200811439](https://doi.org/10.1051/0004-6361/200811439)
- de Mink, S. E., Langer, N., Izzard, R. G., Sana, H., & de Koter, A. 2013, *ApJ*, 764, 166, doi: [10.1088/0004-637X/764/2/166](https://doi.org/10.1088/0004-637X/764/2/166)
- deBoer, R. J., Görres, J., Wiescher, M., et al. 2017, *Reviews of Modern Physics*, 89, 035007, doi: [10.1103/RevModPhys.89.035007](https://doi.org/10.1103/RevModPhys.89.035007)
- Deckers, M., Groh, J. H., Boian, I., & Farrell, E. J. 2021, *MNRAS*, 507, 3726, doi: [10.1093/mnras/stab2423](https://doi.org/10.1093/mnras/stab2423)
- Diehl, R., Korn, A. J., Leibundgut, B., Lugaro, M., & Wallner, A. 2022, *Progress in Particle and Nuclear Physics*, 127, 103983, doi: [10.1016/j.pnpnp.2022.103983](https://doi.org/10.1016/j.pnpnp.2022.103983)
- Diehl, R., Lang, M. G., Martin, P., et al. 2010, *A&A*, 522, A51, doi: [10.1051/0004-6361/201014302](https://doi.org/10.1051/0004-6361/201014302)
- Dominik, M., Belczynski, K., Fryer, C., et al. 2012, *ApJ*, 759, 52, doi: [10.1088/0004-637X/759/1/52](https://doi.org/10.1088/0004-637X/759/1/52)
- . 2013, *ApJ*, 779, 72, doi: [10.1088/0004-637X/779/1/72](https://doi.org/10.1088/0004-637X/779/1/72)
- Eggleton, P. P. 1983, *ApJ*, 268, 368, doi: [10.1086/160960](https://doi.org/10.1086/160960)
- Eitner, P., Bergemann, M., Ruiter, A. J., et al. 2022, arXiv e-prints, arXiv:2206.10258. <https://arxiv.org/abs/2206.10258>
- Ekström, S., Georgy, C., Eggenberger, P., et al. 2012, *A&A*, 537, A146, doi: [10.1051/0004-6361/201117751](https://doi.org/10.1051/0004-6361/201117751)

- Eldridge, J. J., Izzard, R. G., & Tout, C. A. 2008, *MNRAS*, 384, 1109, doi: [10.1111/j.1365-2966.2007.12738.x](https://doi.org/10.1111/j.1365-2966.2007.12738.x)
- Ertl, T., Janka, H. T., Woosley, S. E., Sukhbold, T., & Ugliano, M. 2016, *ApJ*, 818, 124, doi: [10.3847/0004-637X/818/2/124](https://doi.org/10.3847/0004-637X/818/2/124)
- Farmer, R. 2018, *rjfarmer/mesaplot*, doi: [10.5281/zenodo.1441329](https://doi.org/10.5281/zenodo.1441329)
- Farmer, R., & Bauer, E. B. 2018, *rjfarmer/pyMesa: Add support for 10398, v1.0.3*, Zenodo, doi: [10.5281/zenodo.1205271](https://doi.org/10.5281/zenodo.1205271)
- Farmer, R., Fields, C. E., Petermann, I., et al. 2016, *ApJS*, 227, 22, doi: [10.3847/1538-4365/227/2/22](https://doi.org/10.3847/1538-4365/227/2/22)
- Farmer, R., Laplace, E., de Mink, S. E., & Justham, S. 2021, *ApJ*, 923, 214, doi: [10.3847/1538-4357/ac2f44](https://doi.org/10.3847/1538-4357/ac2f44)
- Farmer, R., Renzo, M., de Mink, S. E., Fishbach, M., & Justham, S. 2020, *ApJL*, 902, L36, doi: [10.3847/2041-8213/abbadd](https://doi.org/10.3847/2041-8213/abbadd)
- Ferguson, J. W., Alexander, D. R., Allard, F., et al. 2005, *ApJ*, 623, 585, doi: [10.1086/428642](https://doi.org/10.1086/428642)
- Fields, C. E., Farmer, R., Petermann, I., Iliadis, C., & Timmes, F. X. 2016, *ApJ*, 823, 46, doi: [10.3847/0004-637X/823/1/46](https://doi.org/10.3847/0004-637X/823/1/46)
- Fields, C. E., Timmes, F. X., Farmer, R., et al. 2018, *The Astrophysical Journal Supplement Series*, 234, 19, doi: [10.3847/1538-4365/aaa29b](https://doi.org/10.3847/1538-4365/aaa29b)
- Franchini, M., Morossi, C., Di Marcantonio, P., et al. 2020, *ApJ*, 888, 55, doi: [10.3847/1538-4357/ab5dc4](https://doi.org/10.3847/1538-4357/ab5dc4)
- Franco, M., Coppin, K. E. K., Geach, J. E., et al. 2021, *Nature Astronomy*, 5, 1240, doi: [10.1038/s41550-021-01515-9](https://doi.org/10.1038/s41550-021-01515-9)
- Freiburghaus, C., Rosswog, S., & Thielemann, F. K. 1999, *ApJL*, 525, L121, doi: [10.1086/312343](https://doi.org/10.1086/312343)
- Fuller, G. M., Fowler, W. A., & Newman, M. J. 1985, *ApJ*, 293, 1, doi: [10.1086/163208](https://doi.org/10.1086/163208)
- Gaia Collaboration, Brown, A. G. A., Vallenari, A., et al. 2021, *A&A*, 649, A1, doi: [10.1051/0004-6361/202039657](https://doi.org/10.1051/0004-6361/202039657)
- Gaia Collaboration, Recio-Blanco, A., Kordopatis, G., et al. 2022, *arXiv e-prints*, arXiv:2206.05534. <https://arxiv.org/abs/2206.05534>
- Gallino, R., Arlandini, C., Busso, M., et al. 1998, *ApJ*, 497, 388, doi: [10.1086/305437](https://doi.org/10.1086/305437)
- Goldberg, J. A., Bildsten, L., & Paxton, B. 2019, *ApJ*, 879, 3, doi: [10.3847/1538-4357/ab22b6](https://doi.org/10.3847/1538-4357/ab22b6)
- Goriely, S., Jorissen, A., & Arnould, M. 1990, in *Nuclear Astrophysics, 5th Workshop*, 60
- Götberg, Y., de Mink, S. E., & Groh, J. H. 2017, *A&A*, 608, A11, doi: [10.1051/0004-6361/201730472](https://doi.org/10.1051/0004-6361/201730472)
- Grevesse, N., & Sauval, A. J. 1998, *SSRv*, 85, 161, doi: [10.1023/A:1005161325181](https://doi.org/10.1023/A:1005161325181)
- Griffith, E. J., Sukhbold, T., Weinberg, D. H., et al. 2021, *ApJ*, 921, 73, doi: [10.3847/1538-4357/ac1bac](https://doi.org/10.3847/1538-4357/ac1bac)
- Groh, J. H., Ekström, S., Georgy, C., et al. 2019, *A&A*, 627, A24, doi: [10.1051/0004-6361/201833720](https://doi.org/10.1051/0004-6361/201833720)
- Habets, G. M. H. J. 1986, *A&A*, 165, 95
- Heger, A., Fryer, C. L., Woosley, S. E., Langer, N., & Hartmann, D. H. 2003, *ApJ*, 591, 288, doi: [10.1086/375341](https://doi.org/10.1086/375341)
- Heger, A., & Woosley, S. E. 2002, *ApJ*, 567, 532, doi: [10.1086/338487](https://doi.org/10.1086/338487)
- Heger, A., Woosley, S. E., Martínez-Pinedo, G., & Langanke, K. 2001, *ApJ*, 560, 307, doi: [10.1086/324092](https://doi.org/10.1086/324092)
- Heger, A., Woosley, S. E., Rauscher, T., Hoffman, R. D., & Boyes, M. M. 2002, *NewAR*, 46, 463, doi: [10.1016/S1387-6473\(02\)00184-7](https://doi.org/10.1016/S1387-6473(02)00184-7)
- Herwig, F. 2005, *ARA&A*, 43, 435, doi: [10.1146/annurev.astro.43.072103.150600](https://doi.org/10.1146/annurev.astro.43.072103.150600)
- Hunter, I., Dufton, P. L., Smartt, S. J., et al. 2007, *A&A*, 466, 277, doi: [10.1051/0004-6361:20066148](https://doi.org/10.1051/0004-6361:20066148)
- Hunter, I., Brott, I., Lennon, D. J., et al. 2008, *ApJL*, 676, L29, doi: [10.1086/587436](https://doi.org/10.1086/587436)
- Hunter, I., Brott, I., Langer, N., et al. 2009, *A&A*, 496, 841, doi: [10.1051/0004-6361/200809925](https://doi.org/10.1051/0004-6361/200809925)
- Hunter, J. D. 2007, *Computing In Science & Engineering*, 9, 90
- Iglesias, C. A., & Rogers, F. J. 1993, *ApJ*, 412, 752, doi: [10.1086/172958](https://doi.org/10.1086/172958)
- . 1996, *ApJ*, 464, 943, doi: [10.1086/177381](https://doi.org/10.1086/177381)
- Imasheva, L., Janka, H.-T., & Weiss, A. 2023, *MNRAS*, 518, 1818, doi: [10.1093/mnras/stac3239](https://doi.org/10.1093/mnras/stac3239)
- Itoh, N., Hayashi, H., Nishikawa, A., & Kohyama, Y. 1996, *ApJS*, 102, 411, doi: [10.1086/192264](https://doi.org/10.1086/192264)
- Ivanova, N., & Podsiadlowski, P. 2003, in *From Twilight to Highlight: The Physics of Supernovae*, ed. W. Hillebrandt & B. Leibundgut, 19, doi: [10.1007/10828549_3](https://doi.org/10.1007/10828549_3)
- Iwamoto, K., Brachwitz, F., Nomoto, K., et al. 1999, *ApJS*, 125, 439, doi: [10.1086/313278](https://doi.org/10.1086/313278)
- Izzard, R. G. 2004, PhD thesis, University of Cambridge, UK
- Izzard, R. G., Dray, L. M., Karakas, A. I., Lugaro, M., & Tout, C. A. 2006, *A&A*, 460, 565, doi: [10.1051/0004-6361:20066129](https://doi.org/10.1051/0004-6361:20066129)
- Janssens, S., Shenar, T., Mahy, L., et al. 2021, *A&A*, 646, A33, doi: [10.1051/0004-6361/202039305](https://doi.org/10.1051/0004-6361/202039305)
- Jermyn, A. S., Bauer, E. B., Schwab, J., et al. 2022, *arXiv e-prints*, arXiv:2208.03651. <https://arxiv.org/abs/2208.03651>
- Johnson, J. W., & Weinberg, D. H. 2020, *MNRAS*, 498, 1364, doi: [10.1093/mnras/staa2431](https://doi.org/10.1093/mnras/staa2431)

- Johnson, J. W., Weinberg, D. H., Vincenzo, F., et al. 2021, *MNRAS*, 508, 4484, doi: [10.1093/mnras/stab2718](https://doi.org/10.1093/mnras/stab2718)
- Jones, S., Andrassy, R., Sandalski, S., et al. 2017, *MNRAS*, 465, 2991, doi: [10.1093/mnras/stw2783](https://doi.org/10.1093/mnras/stw2783)
- José, J., Coc, A., & Hernanz, M. 1999, *ApJ*, 520, 347, doi: [10.1086/307445](https://doi.org/10.1086/307445)
- José, J., & Iliadis, C. 2011, *Reports on Progress in Physics*, 74, 096901, doi: [10.1088/0034-4885/74/9/096901](https://doi.org/10.1088/0034-4885/74/9/096901)
- Justham, S., Podsiadlowski, P., & Vink, J. S. 2014, *ApJ*, 796, 121, doi: [10.1088/0004-637X/796/2/121](https://doi.org/10.1088/0004-637X/796/2/121)
- Karakas, A. I. 2010, *MNRAS*, 403, 1413, doi: [10.1111/j.1365-2966.2009.16198.x](https://doi.org/10.1111/j.1365-2966.2009.16198.x)
- Karakas, A. I., & Lugaro, M. 2016, *ApJ*, 825, 26, doi: [10.3847/0004-637X/825/1/26](https://doi.org/10.3847/0004-637X/825/1/26)
- Kasen, D., Metzger, B., Barnes, J., Quataert, E., & Ramirez-Ruiz, E. 2017, *Nature*, 551, 80, doi: [10.1038/nature24453](https://doi.org/10.1038/nature24453)
- Kippenhahn, R., & Weigert, A. 1967, *ZA*, 65, 251
- Klencki, J., Istrate, A., Nelemans, G., & Pols, O. 2022, *A&A*, 662, A56, doi: [10.1051/0004-6361/202142701](https://doi.org/10.1051/0004-6361/202142701)
- Klencki, J., Nelemans, G., Istrate, A. G., & Pols, O. 2020, *A&A*, 638, A55, doi: [10.1051/0004-6361/202037694](https://doi.org/10.1051/0004-6361/202037694)
- Kluyver, T., Ragan-Kelley, B., Pérez, F., et al. 2016, in *Positioning and Power in Academic Publishing: Players, Agents and Agendas: Proceedings of the 20th International Conference on Electronic Publishing*, ed. F. Loizides & B. Schmidt, Amsterdam: IOS Press, 87
- Kobayashi, C., Karakas, A. I., & Lugaro, M. 2020, *ApJ*, 900, 179, doi: [10.3847/1538-4357/abae65](https://doi.org/10.3847/1538-4357/abae65)
- Kolb, U., & Ritter, H. 1990, *A&A*, 236, 385
- Kudritzki, R.-P., & Puls, J. 2000, *ARA&A*, 38, 613, doi: [10.1146/annurev.astro.38.1.613](https://doi.org/10.1146/annurev.astro.38.1.613)
- Kunz, R., Fey, M., Jaeger, M., et al. 2002, *ApJ*, 567, 643, doi: [10.1086/338384](https://doi.org/10.1086/338384)
- Langanke, K., & Martínez-Pinedo, G. 2000, *Nuclear Physics A*, 673, 481, doi: [10.1016/S0375-9474\(00\)00131-7](https://doi.org/10.1016/S0375-9474(00)00131-7)
- Langer, N. 2012, *ARA&A*, 50, 107, doi: [10.1146/annurev-astro-081811-125534](https://doi.org/10.1146/annurev-astro-081811-125534)
- Laplace, E., Göteborg, Y., de Mink, S. E., Justham, S., & Farmer, R. 2020, *A&A*, 637, A6, doi: [10.1051/0004-6361/201937300](https://doi.org/10.1051/0004-6361/201937300)
- Laplace, E., Justham, S., Renzo, M., et al. 2021, *A&A*, 656, A58, doi: [10.1051/0004-6361/202140506](https://doi.org/10.1051/0004-6361/202140506)
- Leising, M. D., & Share, G. H. 1994, *ApJ*, 424, 200, doi: [10.1086/173883](https://doi.org/10.1086/173883)
- Leung, S.-C., & Nomoto, K. 2020, *ApJ*, 888, 80, doi: [10.3847/1538-4357/ab5c1f](https://doi.org/10.3847/1538-4357/ab5c1f)
- Lian, J., Zasowski, G., Mackereth, T., et al. 2022, *MNRAS*, 513, 4130, doi: [10.1093/mnras/stac1151](https://doi.org/10.1093/mnras/stac1151)
- Limongi, M., & Chieffi, A. 2006, *ApJ*, 647, 483, doi: [10.1086/505164](https://doi.org/10.1086/505164)
- . 2018, *ApJS*, 237, 13, doi: [10.3847/1538-4365/aacb24](https://doi.org/10.3847/1538-4365/aacb24)
- Lugaro, M., de Mink, S. E., Izzard, R. G., et al. 2008, *A&A*, 484, L27, doi: [10.1051/0004-6361:20079169](https://doi.org/10.1051/0004-6361:20079169)
- Maeder, A. 1992, *A&A*, 264, 105
- Mahoney, W. A., Ling, J. C., Jacobson, A. S., & Lingenfelter, R. E. 1982, *ApJ*, 262, 742, doi: [10.1086/160469](https://doi.org/10.1086/160469)
- Majewski, S. R., Schiavon, R. P., Frinchaboy, P. M., et al. 2017, *AJ*, 154, 94, doi: [10.3847/1538-3881/aa784d](https://doi.org/10.3847/1538-3881/aa784d)
- Mason, B. D., Hartkopf, W. I., Gies, D. R., Henry, T. J., & Helsel, J. W. 2009, *AJ*, 137, 3358, doi: [10.1088/0004-6256/137/2/3358](https://doi.org/10.1088/0004-6256/137/2/3358)
- Meynet, G., & Arnould, M. 2000, *A&A*, 355, 176, <https://arxiv.org/abs/astro-ph/0001170>
- Meynet, G., Ekström, S., & Maeder, A. 2006, *A&A*, 447, 623, doi: [10.1051/0004-6361:20053070](https://doi.org/10.1051/0004-6361:20053070)
- Meynet, G., & Maeder, A. 2000, *A&A*, 361, 101, <https://arxiv.org/abs/astro-ph/0006404>
- Milam, S. N., Savage, C., Brewster, M. A., Ziurys, L. M., & Wyckoff, S. 2005, *ApJ*, 634, 1126, doi: [10.1086/497123](https://doi.org/10.1086/497123)
- Misch, G. W., Sprouse, T. M., Mumpower, M. R., et al. 2021, *Symmetry*, 13, 1831, doi: [10.3390/sym13101831](https://doi.org/10.3390/sym13101831)
- Moe, M., & Di Stefano, R. 2017, *ApJS*, 230, 15, doi: [10.3847/1538-4365/aa6fb6](https://doi.org/10.3847/1538-4365/aa6fb6)
- Murphy, L. J., Groh, J. H., Ekström, S., et al. 2021, *MNRAS*, 501, 2745, doi: [10.1093/mnras/staa3803](https://doi.org/10.1093/mnras/staa3803)
- Nissen, P. E., Chen, Y. Q., Carigi, L., Schuster, W. J., & Zhao, G. 2014, *A&A*, 568, A25, doi: [10.1051/0004-6361/201424184](https://doi.org/10.1051/0004-6361/201424184)
- Nomoto, K., Iwamoto, K., Nakasato, N., et al. 1997, *NuPhA*, 621, 467, doi: [10.1016/S0375-9474\(97\)00291-1](https://doi.org/10.1016/S0375-9474(97)00291-1)
- Nomoto, K., Kobayashi, C., & Tominaga, N. 2013, *ARA&A*, 51, 457, doi: [10.1146/annurev-astro-082812-140956](https://doi.org/10.1146/annurev-astro-082812-140956)
- Nugis, T., & Lamers, H. J. G. L. M. 2000, *A&A*, 360, 227
- O'Connor, E., & Ott, C. D. 2011, *ApJ*, 730, 70
- Oda, T., Hino, M., Muto, K., Takahara, M., & Sato, K. 1994, *Atomic Data and Nuclear Data Tables*, 56, 231, doi: [10.1006/adnd.1994.1007](https://doi.org/10.1006/adnd.1994.1007)
- Paczyński, B. 1967, *AcA*, 17, 355
- Pagel, B. E. J., & Tautvaisiene, G. 1997, *MNRAS*, 288, 108, doi: [10.1093/mnras/288.1.108](https://doi.org/10.1093/mnras/288.1.108)
- Patton, R. A., & Sukhbold, T. 2020, *MNRAS*, doi: [10.1093/mnras/staa3029](https://doi.org/10.1093/mnras/staa3029)
- Paxton, B., Bildsten, L., Dotter, A., et al. 2011, *ApJS*, 192, 3, doi: [10.1088/0067-0049/192/1/3](https://doi.org/10.1088/0067-0049/192/1/3)
- Paxton, B., Cantiello, M., Arras, P., et al. 2013, *ApJS*, 208, 4, doi: [10.1088/0067-0049/208/1/4](https://doi.org/10.1088/0067-0049/208/1/4)

- Paxton, B., Marchant, P., Schwab, J., et al. 2015, *ApJS*, 220, 15, doi: [10.1088/0067-0049/220/1/15](https://doi.org/10.1088/0067-0049/220/1/15)
- Paxton, B., Schwab, J., Bauer, E. B., et al. 2018, *ApJS*, 234, 34, doi: [10.3847/1538-4365/aaa5a8](https://doi.org/10.3847/1538-4365/aaa5a8)
- Paxton, B., Smolec, R., Schwab, J., et al. 2019, *ApJS*, 243, 10, doi: [10.3847/1538-4365/ab2241](https://doi.org/10.3847/1538-4365/ab2241)
- Peebles, P. J. 1966, *PhRvL*, 16, 410, doi: [10.1103/PhysRevLett.16.410](https://doi.org/10.1103/PhysRevLett.16.410)
- Pérez, F., & Granger, B. E. 2007, *Computing in Science & Engineering*, 9, 21
- Perryman, M. A. C., de Boer, K. S., Gilmore, G., et al. 2001, *A&A*, 369, 339, doi: [10.1051/0004-6361:20010085](https://doi.org/10.1051/0004-6361:20010085)
- Pian, E., D'Avanzo, P., Benetti, S., et al. 2017, *Nature*, 551, 67, doi: [10.1038/nature24298](https://doi.org/10.1038/nature24298)
- Pignatari, M., Herwig, F., Hirschi, R., et al. 2016, *ApJS*, 225, 24, doi: [10.3847/0067-0049/225/2/24](https://doi.org/10.3847/0067-0049/225/2/24)
- Podsiadlowski, P., Joss, P. C., & Hsu, J. J. L. 1992, *ApJ*, 391, 246, doi: [10.1086/171341](https://doi.org/10.1086/171341)
- Podsiadlowski, P., Langer, N., Poelarends, A. J. T., et al. 2004, *ApJ*, 612, 1044, doi: [10.1086/421713](https://doi.org/10.1086/421713)
- Pols, O. R., Tout, C. A., Eggleton, P. P., & Han, Z. 1995a, *MNRAS*, 274, 964, doi: [10.1093/mnras/274.3.964](https://doi.org/10.1093/mnras/274.3.964)
- . 1995b, *MNRAS*, 274, 964, doi: [10.1093/mnras/274.3.964](https://doi.org/10.1093/mnras/274.3.964)
- Potekhin, A. Y., & Chabrier, G. 2010, *Contributions to Plasma Physics*, 50, 82, doi: [10.1002/ctpp.201010017](https://doi.org/10.1002/ctpp.201010017)
- Prantzos, N., Abia, C., Cristallo, S., Limongi, M., & Chieffi, A. 2020, *MNRAS*, 491, 1832, doi: [10.1093/mnras/stz3154](https://doi.org/10.1093/mnras/stz3154)
- Prantzos, N., Arnould, M., & Arcoragi, J. P. 1987, *ApJ*, 315, 209, doi: [10.1086/165125](https://doi.org/10.1086/165125)
- Rauscher, T., Heger, A., Hoffman, R. D., & Woosley, S. E. 2002, *ApJ*, 576, 323, doi: [10.1086/341728](https://doi.org/10.1086/341728)
- Reichert, M., Obergaulinger, M., Aloy, M. Á., et al. 2023, *MNRAS*, 518, 1557, doi: [10.1093/mnras/stac3185](https://doi.org/10.1093/mnras/stac3185)
- Renda, A., Fenner, Y., Gibson, B. K., et al. 2004, *MNRAS*, 354, 575, doi: [10.1111/j.1365-2966.2004.08215.x](https://doi.org/10.1111/j.1365-2966.2004.08215.x)
- Renzo, M., Ott, C. D., Shore, S. N., & de Mink, S. E. 2017, *A&A*, 603, A118, doi: [10.1051/0004-6361/201730698](https://doi.org/10.1051/0004-6361/201730698)
- Renzo, M., Zapartas, E., Justham, S., et al. 2022, *arXiv e-prints*, arXiv:2206.15338, <https://arxiv.org/abs/2206.15338>
- Rizzuti, F., Cescutti, G., Matteucci, F., et al. 2019, *MNRAS*, 489, 5244, doi: [10.1093/mnras/stz2505](https://doi.org/10.1093/mnras/stz2505)
- . 2021, *MNRAS*, 502, 2495, doi: [10.1093/mnras/stab158](https://doi.org/10.1093/mnras/stab158)
- Rogers, F. J., & Nayfonov, A. 2002, *ApJ*, 576, 1064, doi: [10.1086/341894](https://doi.org/10.1086/341894)
- Rohatgi, A. 2022, *Webplotdigitizer: Version 4.6*, <https://automeris.io/WebPlotDigitizer>
- Romano, D., Matteucci, F., Zhang, Z.-Y., Ivison, R. J., & Ventura, P. 2019, *MNRAS*, 490, 2838, doi: [10.1093/mnras/stz2741](https://doi.org/10.1093/mnras/stz2741)
- Saito, S., Tanaka, M., Sawada, R., & Moriya, T. J. 2022, *ApJ*, 931, 153, doi: [10.3847/1538-4357/ac6bec](https://doi.org/10.3847/1538-4357/ac6bec)
- Sallaska, A. L., Iliadis, C., Champange, A. E., et al. 2013, *The Astrophysical Journal Supplement Series*, 207, 18, doi: [10.1088/0067-0049/207/1/18](https://doi.org/10.1088/0067-0049/207/1/18)
- Salpeter, E. E. 1954, *Australian Journal of Physics*, 7, 373, doi: [10.1071/PH540373](https://doi.org/10.1071/PH540373)
- Sana, H., de Mink, S. E., de Koter, A., et al. 2012, *Science*, 337, 444, doi: [10.1126/science.1223344](https://doi.org/10.1126/science.1223344)
- Sander, A. A. C., & Vink, J. S. 2020, *MNRAS*, 499, 873, doi: [10.1093/mnras/staa2712](https://doi.org/10.1093/mnras/staa2712)
- Sander, A. A. C., Vink, J. S., & Hamann, W. R. 2020, *MNRAS*, 491, 4406, doi: [10.1093/mnras/stz3064](https://doi.org/10.1093/mnras/stz3064)
- Saumon, D., Chabrier, G., & van Horn, H. M. 1995, *ApJS*, 99, 713, doi: [10.1086/192204](https://doi.org/10.1086/192204)
- Sawada, R., & Maeda, K. 2019, *ApJ*, 886, 47, doi: [10.3847/1538-4357/ab4da3](https://doi.org/10.3847/1538-4357/ab4da3)
- Schneider, F. R. N., Podsiadlowski, P., & Müller, B. 2021, *A&A*, 645, A5, doi: [10.1051/0004-6361/202039219](https://doi.org/10.1051/0004-6361/202039219)
- Schneider, F. R. N., Sana, H., Evans, C. J., et al. 2018, *Science*, 359, 69, doi: [10.1126/science.aan0106](https://doi.org/10.1126/science.aan0106)
- Schwab, J. 2020, *ApJL*, 901, L18, doi: [10.3847/2041-8213/abb45f](https://doi.org/10.3847/2041-8213/abb45f)
- Sen, K., Langer, N., Marchant, P., et al. 2022, *A&A*, 659, A98, doi: [10.1051/0004-6361/202142574](https://doi.org/10.1051/0004-6361/202142574)
- Sieverding, A., Randhawa, J. S., Zetterberg, D., et al. 2022, *PhRvC*, 106, 015803, doi: [10.1103/PhysRevC.106.015803](https://doi.org/10.1103/PhysRevC.106.015803)
- Simonucci, S., Taioli, S., Palmerini, S., & Busso, M. 2013, *ApJ*, 764, 118, doi: [10.1088/0004-637X/764/2/118](https://doi.org/10.1088/0004-637X/764/2/118)
- Smith, N. 2014, *ARA&A*, 52, 487, doi: [10.1146/annurev-astro-081913-040025](https://doi.org/10.1146/annurev-astro-081913-040025)
- Subedi, S. K., Meisel, Z., & Merz, G. 2020, *ApJ*, 898, 5, doi: [10.3847/1538-4357/ab9745](https://doi.org/10.3847/1538-4357/ab9745)
- Sukhbold, T., & Adams, S. 2020, *MNRAS*, 492, 2578, doi: [10.1093/mnras/staa059](https://doi.org/10.1093/mnras/staa059)
- Sukhbold, T., Ertl, T., Woosley, S. E., Brown, J. M., & Janka, H. T. 2016, *ApJ*, 821, 38, doi: [10.3847/0004-637X/821/1/38](https://doi.org/10.3847/0004-637X/821/1/38)
- Sukhbold, T., & Woosley, S. E. 2014, *ApJ*, 783, 10, doi: [10.1088/0004-637X/783/1/10](https://doi.org/10.1088/0004-637X/783/1/10)
- Tange, O. 2021, *GNU Parallel 20211222 ('Støjberg')*, Zenodo, doi: [10.5281/zenodo.5797028](https://doi.org/10.5281/zenodo.5797028)
- Tanvir, N. R., Levan, A. J., González-Fernández, C., et al. 2017, *ApJL*, 848, L27, doi: [10.3847/2041-8213/aa90b6](https://doi.org/10.3847/2041-8213/aa90b6)
- Timmes, F., Fryer, C., Timmes, F., et al. 2019, *BAAS*, 51, 2, <https://arxiv.org/abs/1902.02915>
- Timmes, F. X., & Swesty, F. D. 2000, *ApJS*, 126, 501, doi: [10.1086/313304](https://doi.org/10.1086/313304)
- Timmes, F. X., Woosley, S. E., & Weaver, T. A. 1996, *ApJ*, 457, 834, doi: [10.1086/176778](https://doi.org/10.1086/176778)

- Tinsley, B. M. 1980, *FCPh*, 5, 287,
doi: [10.48550/arXiv.2203.02041](https://doi.org/10.48550/arXiv.2203.02041)
- Tout, C. A., Pols, O. R., Eggleton, P. P., & Han, Z. 1996,
MNRAS, 281, 257, doi: [10.1093/mnras/281.1.257](https://doi.org/10.1093/mnras/281.1.257)
- Townsend, R. 2019, *MESA SDK for Linux*: 20190911,
doi: [10.5281/zenodo.2603170](https://doi.org/10.5281/zenodo.2603170)
- Ugliano, M., Janka, H.-T., Marek, A., & Arcones, A. 2012,
ApJ, 757, 69, doi: [10.1088/0004-637X/757/1/69](https://doi.org/10.1088/0004-637X/757/1/69)
- van den Heuvel, E. P. J. 1969, *AJ*, 74, 1095,
doi: [10.1086/110909](https://doi.org/10.1086/110909)
- van den Hoek, L. B., & Groenewegen, M. A. T. 1997,
A&AS, 123, 305, doi: [10.1051/aas:1997162](https://doi.org/10.1051/aas:1997162)
- van der Walt, S., Colbert, S. C., & Varoquaux, G. 2011,
Computing in Science Engineering, 13, 22,
doi: [10.1109/MCSE.2011.37](https://doi.org/10.1109/MCSE.2011.37)
- Vink, J. S., de Koter, A., & Lamers, H. J. G. L. M. 2001,
A&A, 369, 574, doi: [10.1051/0004-6361:20010127](https://doi.org/10.1051/0004-6361:20010127)
- Wagoner, R. V., Fowler, W. A., & Hoyle, F. 1967, *ApJ*,
148, 3, doi: [10.1086/149126](https://doi.org/10.1086/149126)
- Wellstein, S., & Langer, N. 1999, *A&A*, 350, 148.
<https://arxiv.org/abs/astro-ph/9904256>
- West, C., Heger, A., & Austin, S. M. 2013, *ApJ*, 769, 2,
doi: [10.1088/0004-637X/769/1/2](https://doi.org/10.1088/0004-637X/769/1/2)
- Wiescher, M., & Langanke, K. 1986, *Zeitschrift fur Physik
A Hadrons and Nuclei*, 325, 309,
doi: [10.1007/BF01294614](https://doi.org/10.1007/BF01294614)
- Winteler, C., Käppeli, R., Perego, A., et al. 2012, *ApJL*,
750, L22, doi: [10.1088/2041-8205/750/1/L22](https://doi.org/10.1088/2041-8205/750/1/L22)
- Woosley, S. E. 2018, *ApJ*, 863, 105,
doi: [10.3847/1538-4357/aad044](https://doi.org/10.3847/1538-4357/aad044)
- Woosley, S. E., & Haxton, W. C. 1988, *Nature*, 334, 45,
doi: [10.1038/334045a0](https://doi.org/10.1038/334045a0)
- Woosley, S. E., & Heger, A. 2007, *PhR*, 442, 269,
doi: [10.1016/j.physrep.2007.02.009](https://doi.org/10.1016/j.physrep.2007.02.009)
- Woosley, S. E., Heger, A., & Weaver, T. A. 2002, *Rev.
Mod. Phys.*, 74, 1015, doi: [10.1103/RevModPhys.74.1015](https://doi.org/10.1103/RevModPhys.74.1015)
- Woosley, S. E., Langer, N., & Weaver, T. A. 1993, *ApJ*,
411, 823, doi: [10.1086/172886](https://doi.org/10.1086/172886)
- Woosley, S. E., & Weaver, T. A. 1994, *ApJ*, 423, 371,
doi: [10.1086/173813](https://doi.org/10.1086/173813)
- Yoon, S.-C., Dessart, L., & Clocchiatti, A. 2017, *ApJ*, 840,
10, doi: [10.3847/1538-4357/aa6afe](https://doi.org/10.3847/1538-4357/aa6afe)
- Yoon, S. C., Woosley, S. E., & Langer, N. 2010, *ApJ*, 725,
940, doi: [10.1088/0004-637X/725/1/940](https://doi.org/10.1088/0004-637X/725/1/940)
- Young, P. A., & Fryer, C. L. 2007, *ApJ*, 664, 1033,
doi: [10.1086/518081](https://doi.org/10.1086/518081)
- Zapartas, E., de Mink, S. E., Izzard, R. G., et al. 2017,
A&A, 601, A29, doi: [10.1051/0004-6361/201629685](https://doi.org/10.1051/0004-6361/201629685)
- Zapartas, E., de Mink, S. E., Justham, S., et al. 2019,
A&A, 631, A5, doi: [10.1051/0004-6361/201935854](https://doi.org/10.1051/0004-6361/201935854)